The sections (5 sections/animal) were quantitatively analyzed using a confocal laser scanning microscope (Leica TCS-SP5, Leica Microsystems, Mannhein, Germany), at a magnification of 20×. The obtained images were imported into the MetaMorph software program (Molecular Devices, Downingtown, PA) and the threshold tool of this program was used to isolate c-Fos-immunopositive and DAPI-labeled cells, which cells were counted in a genotype-blind manner.

### In vivo microdialysis

The mice were anesthetized with sodium pentobarbital before the stereotactic implantation of a probe into the left hilus of DG (−1.8 mm anteroposterior, +1.8 mm mediolateral from the bregma, and −2 mm dorsoventral with respect to the dura). Probes were secured onto the skull using stainless-steel screws and dental acrylic. Twenty-four hours after the surgery, in vivo microdialysis was performed on conscious mice. Probes were perfused continuously with artificial cerebrospinal fluid (CSF, 147 mM NaCl, 4 mM KCl, and 2.3 mM $CaCl_2$) at a rate of 2 μL/min. PTZ at 50 mg/kg was injected intraperitoneally at 0 min as indicated in Fig. 3, and the dialysate was collected in 30 min fractions, and then stored at −80 °C until use.

### Measurement of amino acids

Total serine, D-serine, and L-serine levels were measured using a column-switching high-performance liquid chromatography (HPLC) system (Shimadzu Corporation, Kyoto, Japan) as previously reported (Fukushima et al., 2004; Yamada et al., 2005). Glutamate level was measured using an HPLC system with fluorescence detection, as previously reported (Hashimoto et al., 2005).

A 20-μL aliquot of the resultant solution was injected into the HPLC system. A reversed-phase ODS column [TSKgel ODS-80Ts (Tosoh Corporation, Tokyo, Japan) as Column 1] was used for the separation and quantification of total D-serine and L-serine, and the gradient elution of the mobile phase was maintained at a constant flow rate of 0.8 mL/min. Mobile phase 1a consisted of $H_2O$/acetonitrile (90/10) containing 0.1% trifluoroacetic acid (TFA), and phases 1b and 1c consisted of $H_2O$/acetonitrile (10/90) containing 0.1% TFA and acetonitrile, respectively. The time program for gradient elution was as follows: 0–25 min 1a:1b:1c = 92:8:0, 25–25.1 min linear gradient from 8% 1b to 100% 1b, 25.1–35 min 1a:1b:1c = 0:100:0, 35–35.1 min linear gradient from 8% 1b to 100% 1c, 35.1–40 min 1a:1b:1c = 0:0:100, and 40.1–60 min 1a:1b:1c = 92:8:0. The chiral column (Column 2) used for the separation and quantification of D-serine and L-serine with NBD-F comprised two Sumichiral OA-2500 columns (S) (Sumika Chemical Analysis Service Ltd., Osaka, Japan), which were connected in tandem. The mobile phase was 15 mM citric acid in methanol and was isocratically pumped at a flow rate of 1.0 mL/min. The column temperature was maintained at 35 °C for all columns. Fluorescence was detected at 530 nm with an excitation wavelength of 470 nm.

For the determination of glutamate level, a reversed-phase ODS column (TSKgel ODS-80Ts, Tosoh Corporation, Tokyo, Japan) was used. The gradient elution of the mobile phase was kept at a constant flow rate of 0.8 mL/min. The time program for gradient elution was as follows: 0–50.5 min 1a:1b:1c = 95:5:0, 50.5–55.5 min 1a:1b:1c = 0:100:0, and 55.5–57 min, 1a:1b:1c = 0:0:100. All the columns were maintained at 35 °C. Fluorescence was detected at 530 nm with an excitation wavelength of 470 nm.

### Statistical analyses

Seizure categorical data were compared using Mann–Whitney's test or Fisher's exact test. The duration of generalized seizures and immunohistochemical data were compared between the two mouse genotypes using two-tailed Student's *t*-test. For in vivo microdialysis, the average level of each amino acid during the period before the PTZ injection (four samples) was used as the baseline control value. The extracellular levels of glutamate at various time points after PTZ injection were expressed as percentages of the baseline levels of glutamate. The statistical significance of difference was examined by two-tailed Student's *t*-test or repeated measures two-way ANOVA. Data are presented as means ± standard errors of mean ($m \pm SEM$). Values of $p < 0.05$ were considered significant.

## Results

### Seizure-related behaviors in WT and SR-KO mice

The doses of 35, 50, and 65 mg/kg PTZ used for this experiment induced seizures in both WT and SR-KO mice in a dose-dependent manner. As shown in Fig. 1A, at the dose of 35 mg/kg PTZ, most of the WT and SR-KO mice exhibited stage 1 (WT, 8 of 8; SR-KO, 7 of 7) and stage 2 (WT, 5 of 8; SR-KO, 4 of 7) seizures, and only a small proportion of the mice (WT, 2 of 8; SR-KO, 2 of 7) exhibited stage 3 seizure. There were no significant differences in the severity of the seizure at this dose between the two genotypes (Mann–Whitney's test, $p = 0.98$). At the dose of 50 mg/kg, all the WT ($n = 12$) and SR-KO mice ($n = 13$) exhibited stage 3 seizures and one WT mouse showed stage 4 seizures and died during seizures (Fig. 1B). At the dose of 65 mg/kg, of thirteen WT mice, all exhibited stage 3 seizures and six exhibited stage 4 seizures, one of which died. In contrast, all the SR-KO mice exhibited stage 3 seizures, but not stage 4 seizures. This difference reached statistical significance (Fig. 1C, Fisher's exact test, $p = 0.007$). In addition, the durations of generalized seizures (stage 3 and stage 4 seizures) in SR-KO mice at the doses of 50 mg/kg (19.3 ± 1.4 s, Fig. 1D) and 65 mg/kg (22.8 ± 2.9 s, Fig. 1E) were significantly shorter than those in WT mice at the same doses (23.5 ± 1.3 s and 38.8 ± 4.2 s, respectively). There were no significant differences in the latency to the onset of seizures induced at the three doses of PTZ between the two genotypes (data not shown).

### c-Fos expression induced by PTZ in the cerebral cortex, hippocampus, and basolateral nucleus of amygdala

To investigate the difference in the neuronal activity in the brain regions involved in the seizures following PTZ injection

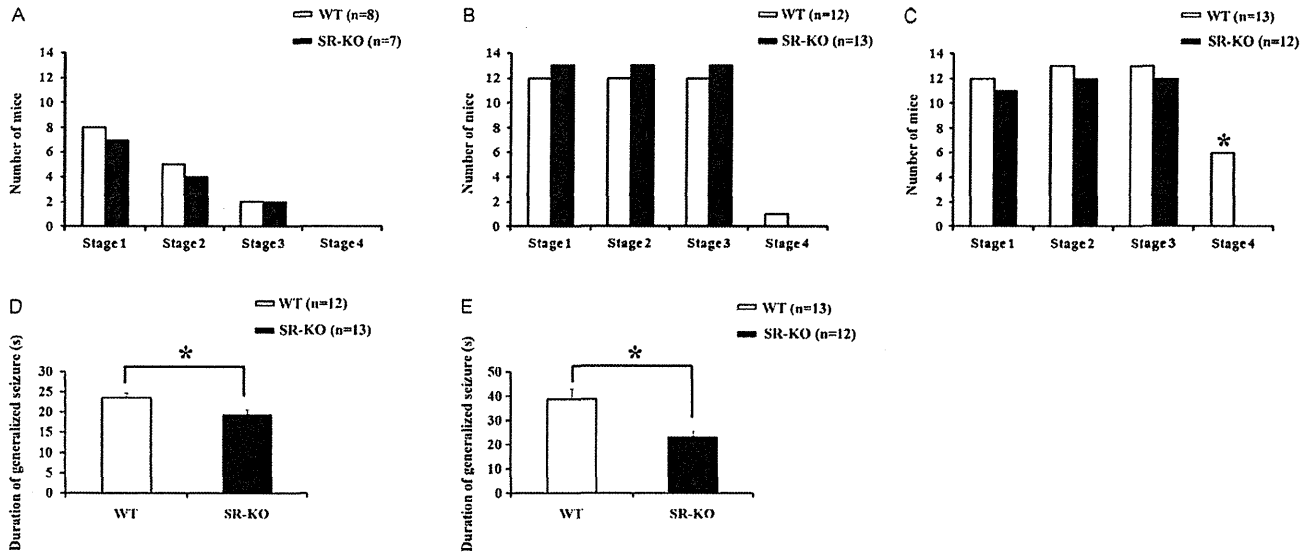


**Figure 1** Pentylenetetrazole (PTZ) induced seizures in wild-type (WT) and SR-KO mice. (A–C) Bar graphs show the number of mice exhibiting stages 1, 2, 3, and 4 seizures after receiving 35 (A), 50 (B), and 65 (C) mg/kg PTZ. Stage 4 seizure induced by 65 mg/kg PTZ was only observed in WT mice, but not in SR-KO mice. This difference is statistically significant. *$p < 0.05$; Fisher's exact test. (D and E) Bar graphs indicate the durations of generalized seizures observed in WT and SR-KO mice after receiving 50 (D), and 65 (E) mg/kg PTZ. SR-KO mice showed significantly shorter durations of generalized seizures (stage 3 and 4 seizures) induced by either 50 or 65 mg/kg PTZ than WT mice. Data are presented as mean ± SEM. *$p < 0.05$; two-tailed Student's $t$-test. $n$ = number of mice.

between WT and SR-KO mice, we examined c-Fos expression by immunohistochemical analysis in the retrosplenial region of the cerebral cortex (Ctx), area CA1, area CA3, hippocampal dentate gyrus (DG), and the basolateral nucleus of the amygdala (BLA) 2 h after injection of PTZ at each dose. We first examined c-Fos immunopositivity in both WT and SR-KO mice under basal conditions, that is, without injection of either saline or PTZ. c-Fos was observed to be expressed in a few cells in all the examined brain regions and there was no significant difference in the number of c-Fos-immunopositive cells between the two genotypes (see Supplementary Fig. 1A). As shown in Supplementary Fig. 1B, the numbers of c-Fos-immunopositive cells in all the examined brain regions of the mice receiving saline injections were comparable to those of the mice under the basal conditions. Injection of 35 mg/kg PTZ induced an increase in the number of c-Fos-immunopositive cells in the Ctx, area CA1, area CA3, and BLA in either WT or SR-KO mice as compared with the saline control, but there was no significant difference in the number of c-Fos-immunopositive cells between the two genotypes at this dose (see Supplementary Fig. 2). An increase in PTZ dose to 50 or 65 mg/kg induced a further increase in the number of c-Fos-immunopositive cells in all of the examined brain regions in both WT and SR-KO mice, and the most marked increase was observed in the hippocampal DG (Fig. 2A and B). At the dose of 50 mg/kg, the percentage of c-Fos-immunopositive cells in the Ctx of WT mice was significantly higher than that of SR-KO mice (Fig. 2C). At the dose of 65 mg/kg, the percentages of c-Fos-immunopositive cells in the Ctx, area CA1, area CA3, and BLA of WT mice were significantly higher than those of SR-KO mice (Fig. 2D).

## Changes in level of extracellular glutamate induced by PTZ injection

As described above, at stages 3 and 4 seizures induced by 50 or 65 mg/kg PTZ, the increase in the number of c-Fos-immunopositive cells was predominantly detected in the hippocampal DG. Therefore, we selected the DG for microdialysis of extracellular glutamate in the group of mice receiving 50 mg/kg PTZ, which was shown to be a sufficient dose for inducing generalized seizures in both WT and SR-KO mice.

The average baseline level of glutamate during the period preceding the PTZ injection (2 h; four measurements every 30 min) was used as the baseline level for the assessment of the changes in the level of glutamate after PTZ injection. As shown in Fig. 3A, under basal conditions, the level of glutamate in the hippocampal DG of SR-KO mice ($0.791 \pm 0.073$ μM) was significantly lower than that of WT mice ($1.315 \pm 0.121$ μM). Regarding the changes in extracellular glutamate level after PTZ injection, ANOVA showed significant main effects of genotype ($F_{1, 146} = 57.73$, $p < 0.001$) and time point ($F_{7, 146} = 4.3$, $p < 0.001$), as well as phenotype × time point interaction ($F_{7, 146} = 7.78$, $p < 0.001$) (Fig. 3B). The post hoc test for the comparison of glutamate level at each time point with the baseline level showed that the glutamate levels in WT mice at 0–30 min and 150–210 min were significantly higher than the baseline level. The early increase was transient, appearing immediately after PTZ injection, and the late increase was gradual, appearing after the termination of convulsive seizures and from 150 to 210 min after PTZ injection. In contrast, glutamate level significantly decreased in SR-KO mice after PTZ

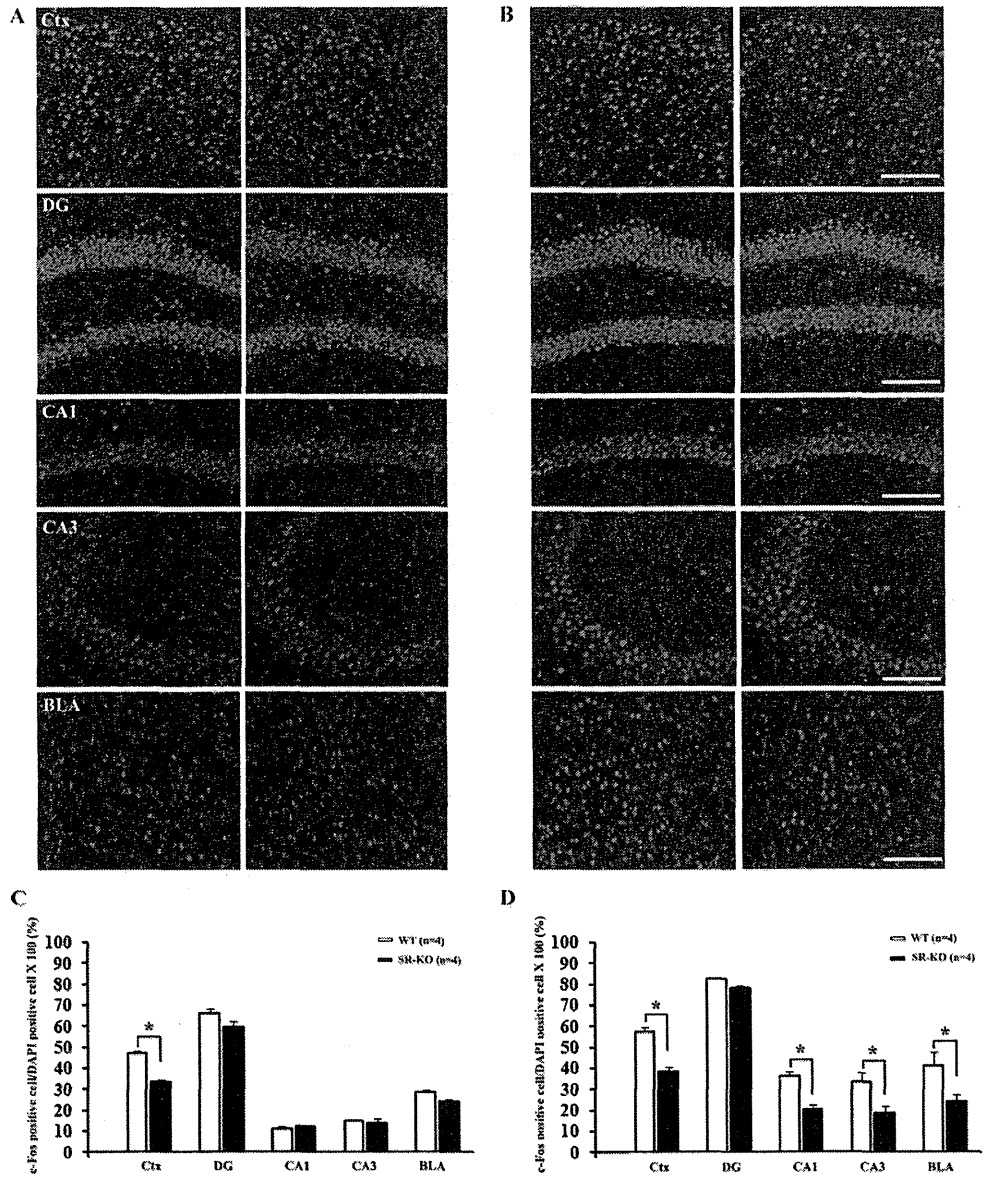


**Figure 2** c-Fos expression induced by PTZ in restrosplenial region of cerebral cortex, hippocampus, and basolateral nucleus of amygdala. Brain sections from WT and SR-KO mice 2 h after 50 mg/kg (A) and 65 mg/kg (B) PTZ injection were subjected to c-Fos immunohistochemical analysis and nuclear labeling with DAPI. The numbers of DAPI-labeled (blue) and c-Fos-immunopositive (magenta) cells in five sections per animal were counted to obtain the percentage of c-Fos-immunopositive cells in the brain regions examined. Bar graphs represent the percentage (mean ± SEM) of the number of c-Fos-immunopositive cells with respect to that of DAPI-positive cells in the brain regions of WT and SR-KO mice receiving 50 mg/kg (C) and 65 mg/kg (D) PTZ. Statistical significance of differences was assessed using two-tailed Student's *t*-test. $^*p < 0.05$. Scale bars: 100 μm. Ctx, cerebral cortex; DG, dentate gyrus; BLA, basolateral nucleus of amygdala. *n* = number of mice.

injection (Fig. 3B). The glutamate levels (% of baseline level) at the time points of 150–180 and 180–210 min after PTZ injection in SR-KO mice were significantly lower than those in WT mice.

We also examined the level of extracellular D-serine in the hippocampal DG of WT and SR-KO mice. As shown in Fig. 3C, under basal conditions, SR-KO mice showed a significantly lower level of extracellular D-serine (0.102 ± 0.004 μM) than WT mice (0.701 ± 0.049 μM).

## Discussion

PTZ induces absence seizures, myoclonic seizures, generalized clonic seizures, and tonic–clonic seizures in a dose-dependent manner (Erbayat-Altay et al., 2008). PTZ models have been used for assessing the anticonvulsant effect of channel-blocking NMDA receptor antagonists and glycine site antagonists (Velísek et al., 1991; Danysz and Parsons, 1998). Therefore, we used PTZ to assess the

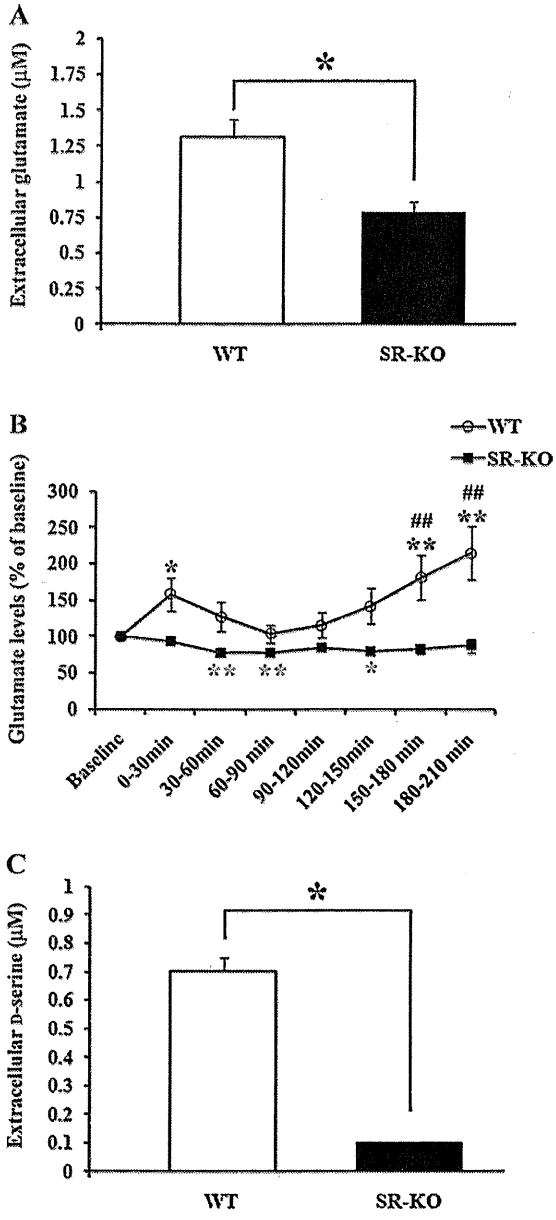


**Figure 3** PTZ-induced change in glutamate level in dentate gyrus of WT and SR-KO mice. (A) Average level of glutamate in dentate gyrus of WT and SR-KO mice before PTZ injection. Data represent mean ± SEM. $^{*}p < 0.05$; two-tailed Student's *t*-test. (B) The average level of glutamate before PTZ injection was used as the baseline control value. PTZ (50 mg/kg) was injected at 0 min and the change in the level of glutamate is presented as the percentage of the baseline level. The extracellular glutamate level was significantly higher than the baseline level after PTZ injection in WT mice, but not in SR-KO mice. Data are expressed as mean ± SEM (7–9 animals per group). Asterisks ($^{*}p < 0.05$ and $^{**}p < 0.01$) denote statistically significant differences compared with the baseline level of glutamate in the same group. Pound signs ($^{\#\#}p < 0.01$) denote statistically significant differences between the two genotypes. (C) Average level of D-serine in dentate gyrus of WT and SR-KO mice before PTZ injection. Data represent mean ± SEM. $^{*}p < 0.05$; two-tailed Student's *t*-test.

anticonvulsant effect of D-serine deficiency in SR-KO mice. We found the resistance of SR-KO mice to generalized clonic–tonic seizures that were induced by 65 mg/kg PTZ, but no marked difference in the occurrence of stages 1 and 2 seizures induced by 35 mg/kg PTZ between the two genotypes. Our findings are in agreement with the study showing that pretreatment with MK-801, a channel-blocking NMDA receptor antagonist, inhibits generalized tonic–clonic seizures and exerts no effect on minimal seizures (stages 1 and 2 seizures) (Velísek et al., 1991). The lower susceptibility of SR-KO mice to PTZ-induced seizures was also shown by the shorter duration of generalized seizures at the dose of either 50 or 65 mg/kg in this genotype than in WT mice. Similarly, one previous study demonstrated a longer duration of generalized tonic-clonic seizures induced by PTZ in NMDA-pretreated mice than in saline-pretreated mice (Stafstrom and Sasaki-Adams, 2003), suggesting that NMDA receptor activity is involved in PTZ-induced generalized seizures. The attenuation of severe-type seizures induced by 65 mg/kg PTZ in SR-KO mice is presumably attributed to the functional impairment of the NMDA receptor by D-serine deficiency, which suggests a possibility of targeting SR as a new therapeutic strategy for epileptic seizures. In addition to the PTZ model, the maximal electroshock seizure (MES) test is also commonly used for assessing the efficacy of an anticonvulsant drug in inhibiting tonic hindlimb extension in mice (Löscher and Schmidt, 1988). Thus, it would be interesting to examine whether D-serine deficiency in SR-KO mice has the anticonvulsant effect in the MES test.

To determine whether there is a significant difference in neuronal activity in the brain between WT and SR-KO mice during seizures, we examined c-Fos expression by immunohistochemical analysis of the Ctx, CA1, CA3, and DG of the hippocampus, and BLA 2 h after PTZ injection. We found no significant difference in the level of c-Fos expression induced by PTZ at 35 mg/kg between the two genotypes. In contrast, the percentages of c-Fos-immunopositive cells in the Ctx, CA1, CA3, and BLA induced by 65 mg/kg PTZ were significantly higher in WT than in SR-KO mice. This finding indirectly indicates that the hyperexcitability of neurons in these areas during generalized seizures is attenuated in SR-KO mice, which putatively contributes to their resistance to the severe type of generalized clonic–tonic seizures.

Glutamate is the most abundant excitatory neurotransmitter in CNS and the dysregulation of its extracellular level contributes to the initiation and spread of seizure activity (Geula et al., 1988; Li et al., 2000; Löscher, 1998; Ueda and Tsuru, 1994). Microdialysis in the hippocampal DG demonstrated significant increases in extracellular glutamate level in the WT mice at two different time points after PTZ injection, as shown by an early rapid increase in the level appearing within 0–30 min after PTZ injection and a late increase appearing after the termination of generalized seizures. Interestingly, such changes were completely suppressed in SR-KO mice. In addition, the baseline level of glutamate in SR-KO mice was lower than that in WT mice. Although there has been a lack of direct evidence for the mechanism(s) by which D-serine participates in the regulation of extracellular glutamate level in the brain, two recent studies might provide clues to understanding the role of D-serine in this aspect. In addition to its location at the postsynaptic density, the NMDA receptor was also

found in presynaptic terminals (Corlew et al., 2008). Furthermore, in the rat visual cortex, the glycine binding site of the presynaptic NMDA receptor was found to be involved in the regulation of the release of glutamate (Li and Han, 2007). It is likely that in SR-KO mice the deficiency of D-serine, a potent coagonist of the glycine binding site, could impair the function of the presynaptic NMDA receptor and thereby decrease the amount of glutamate released from presynaptic terminals. These notions, together with our findings, suggest that D-serine plays a role in the regulation of extracellular glutamate level in the brain during the development of seizures. We also found that the glutamate level in SR-KO mice significantly decreased after PTZ injection. At present, the mechanism(s) underlying this decrease in glutamate level is unclarified, but the dynamics of glutamate transport regulated by neuronal activity (Benediktsson et al., 2012) may be involved in this process. Further study is required to elucidate the mechanism (s) underlying the role of D-serine in the regulation of extracellular glutamate level in the brain.

## Acknowledgements

We thank Ms. Momoko Kadoshima for help in immunohistochemical analysis. This work was supported by a Grant-in-Aid for Young Scientists (B) from the Japan Society for the Promotion of Science (No. 22700332).

## Appendix A. Supplementary data

Supplementary data associated with this article can be found, in the online version, at http://dx.doi.org/10.1016/j.eplepsyres.2012.06.001.

## References

Benediktsson, A.M., Marrs, G.S., Tu, J.C., Worley, P.F., Rothstein, J.D., Bergles, D.E., Dailey, M.E., 2012. Neuronal activity regulates glutamate transporter dynamics in developing astrocytes. Glia 60, 175–188.

Bliss, T.V.P., Collingridge, G.L., 1993. A synaptic model of memory – long-term potentiation in the hippocampus. Nature 361, 31–39.

Brandt, C., Potschka, H., Loscher, W., Ebert, U., 2003. N-methyl-D-aspartate receptor blockade after status epilepticus protects against limbic brain damage but not against epilepsy in the kainate model of temporal lobe epilepsy. Neuroscience 118, 727–740.

Clifford, D.B., Olney, J.W., Benz, A.M., Fuller, T.A., Zorumski, C.F., 1990. Ketamine, phencyclidine, and MK-801 protect against kainic acid-induced seizure-related brain damage. Epilepsia 31, 382–390.

Cloix, J.F., Hevor, T., 2009. Epilepsy, regulation of brain energy metabolism and neurotransmission. Curr. Med. Chem. 16, 841–853.

Corlew, R., Brasier, D.J., Feldman, D.E., Philpot, B.D., 2008. Presynaptic NMDA receptors: newly appreciated roles in cortical synaptic function and plasticity. Neuroscientist 14, 609–625.

Croucher, M.J., Collins, J.F., Meldrum, B.S., 1982. Anticonvulsant action of excitatory amino acid antagonists. Science 216, 899–901.

Danysz, W., Parsons, C.G., 1998. Glycine and N-methyl-D-aspartate receptors: physiological significance and possible therapeutic applications. Pharmacol Rev. 50, 597–664.

Dingledine, R., Borges, K., Bowie, D., Traynelis, S.F., 1999. The glutamate receptor ion channels. Pharmacol. Rev. 51, 7–61.

Dragunow, M., Robertson, H.A., 1988. Localization and induction of c-fos protein-like immunoreactive material in the nuclei of adult mammalian neurons. Brain Res. 440, 252–260.

During, M.J., Spencer, D.D., 1993. Extracellular hippocampal glutamate and spontaneous seizure in the conscious human brain. Lancet 341, 1607–1610.

Erbayat-Altay, E., Yamada, K.A., Wong, M., Thio, L.L., 2008. Increased severity of pentylenetetrazol induced seizures in leptin deficient ob/ob mice. Neurosci. Lett. 433, 82–86.

Fadda, E., Danysz, W., Wroblewski, J.T., Costa, E., 1988. Glycine and D-serine increase the affinity of N-methyl-D-aspartate sensitive glutamate binding sites in rat brain synaptic membranes. Neuropharmacology 27, 1183–1185.

Ferraro, T.N., Golden, G.T., Smith, G.G., St Jean, P., Schork, N.J., Mulholland, N., Ballas, C., Schill, J., Buono, R.J., Berrettini, W.H., 1999. Mapping loci for pentylenetetrazol-induced seizure susceptibility in mice. J. Neurosci. 19, 6733–6739.

Fisher, R.S., 1989. Animal-models of the epilepsies. Brain Res. Rev. 14, 245–278.

Fukushima, T., Kawai, J., Imai, K., Toyo'oka, T., 2004. Simultaneous determination of D- and L-serine in rat brain microdialysis sample using a column-switching HPLC with fluorimetric detection. Biomed. Chromatogr. 18, 813–819.

Geula, C., Jarvie, P.A., Logan, T.C., Slevin, J.T., 1988. Long-term enhancement of $K^+$-evoked release of L-glutamate in entorhinal kindled rats. Brain Res. 442, 368–372.

Hashimoto, A., Nishikawa, T., Hayashi, T., Fujii, N., Harada, K., Oka, T., Takahashi, K., 1992. The presence of free D-serine in rat brain. FEBS Lett. 296, 33–36.

Hashimoto, K., Engberg, G., Shimizu, E., Nordin, C., Lindstrom, L.H., Iyo, M., 2005. Elevated glutamine/glutamate ratio in cerebrospinal fluid of first episode and drug naive schizophrenic patients. BMC Psychiatry 5, 6.

Herron, C.E., Lester, R.A.J., Coan, E.J., Collingridge, G.L., 1986. Frequency-dependent involvement of NMDA receptors in the hippocampus – a novel synaptic mechanism. Nature 322, 265–268.

Inoue, R., Hashimoto, K., Harai, T., Mori, H., 2008. NMDA- and beta-amyloid1-42-induced neurotoxicity is attenuated in serine racemase knock-out mice. J. Neurosci. 28, 14486–14491.

Kohl, B.K., Dannhardt, G., 2001. The NMDA receptor complex: a promising target for novel antiepileptic strategies. Curr. Med. Chem. 8, 1275–1289.

Li, Y.H., Han, T.Z., 2007. Glycine binding sites of presynaptic NMDA receptors may tonically regulate glutamate release in the rat visual cortex. J. Neurophysiol. 97, 817–823.

Li, Z.Q., Yamamoto, Y., Morimoto, T., Ono, J., Okada, S., Yamatodani, A., 2000. The effect of pentylenetetrazole-kindling on the extracellular glutamate and taurine levels in the frontal cortex of rats. Neurosci. Lett. 282, 117–119.

Löscher, W., Schmidt, D., 1988. Which animal models should be used in the search for new antiepileptic drugs? A proposal based on experimental and clinical considerations. Epilepsy Res. 2, 145–181.

Löscher, W., 1998. Pharmacology of glutamate receptor antagonists in the kindling model of epilepsy. Prog. Neurobiol. 54, 721–741.

Matsui, T., Sekiguchi, M., Hashimoto, A., Tomita, U., Nishikawa, T., Wada, K., 1995. Functional comparison of D-serine and glycine in rodents: the effect on cloned NMDA receptors and the extracellular concentration. J. Neurochem. 65, 454–458.

McCormick, D.A., Contreras, D., 2001. On the cellular and network bases of epileptic seizures. Ann. Rev. Physiol. 63, 815–846.

Meldrum, B.S., 1994. The role of glutamate in epilepsy and other CNS disorders. Neurology 44, 14–23.

Miya, K., Inoue, R., Takata, Y., Abe, M., Natsume, R., Sakimura, K., Hongou, K., Miyawaki, T., Mori, H., 2008. Serine racemase is predominantly localized in neurons in mouse brain. J. Comp. Neurol. 510, 641–654.

Mothet, J.P., Parent, A.T., Wolosker, H., Brady, R.O., Linden, D.J., Ferris, C.D., Rogawski, M.A., Snyder, S.H., 2000. D-Serine is an endogenous ligand for the glycine site of the N-methyl-D-aspartate receptor. Proc. Natl. Acad. Sci. U.S.A. 97, 4926–4931.

Paxinos, G., Franklin, K.B.J., 2001. The Mouse Brain in Stereotaxic Coordinates. Acdemic Press.

Sagar, S.M., Sharp, F.R., Curran, T., 1988. Expression of c-fos protein in brain: metabolic mapping at the cellular level. Science 240, 1328–1331.

Sahai, S., 1990. Glutamate in the mammalian CNS. Eur. Arch. Psychiatry Clin. Neurosci. 240, 121–133.

Stafstrom, C.E., Sasaki-Adams, D.M., 2003. NMDA-induced seizures in developing rats cause long-term learning impairment and increased seizure susceptibility. Epilepsy Res. 53, 129–137.

Ueda, Y., Tsuru, N., 1994. Bilateral seizure-related changes of extracellular glutamate concentration in hippocampi during development of amygdaloid kindling. Epilepsy Res. 18, 85–88.

Velísek, L., Veresová, S., Pôbisová, H., Mares, P., 1991. Excitatory amino acid antagonists and pentylenetetrazol-induced seizures during ontogenesis. II. The effects of MK-801. Psychopharmacology 104, 510–514.

Wolosker, H., Blackshaw, S., Snyder, S.H., 1999. Serine racemase: a glial enzyme synthesizing D-serine to regulate glutamate-N-methyl-D-aspartate neurotransmission. Proc. Natl. Acad. Sci. U.S.A. 96, 13409–13414.

Yamada, K., Ohnishi, T., Hashimoto, K., Ohba, H., Iwayama-Shigeno, Y., Toyoshima, M., Okuno, A., Takao, H., Toyota, T., Minabe, Y., Nakamura, K., Shimizu, E., Itokawa, M., Mori, N., Iyo, M., Yoshikawa, T., 2005. Identification of multiple serine racemase (SRR) mRNA isoforms and genetic analyses of SRR and DAO in schizophrenia and D-serine levels. Biol. Psychiatry 57, 1493–1503.

# A Novel Missense Mutation Causing a G487R Substitution in the S2–S3 Loop of Human *ether-à-go-go*-Related Gene Channel

KOSHI KINOSHITA, PH.D.,* YOSHIAKI YAMAGUCHI, M.D.,†,¶ KOHKI NISHIDE, B.E.,‡,¶ KATSUYA KIMOTO, B.E.,‡ YUKI NONOBE, B.E.,‡ AKIRA FUJITA, B.E.,‡ KENTA ASANO, B.E.,‡ TOSHIHIDE TABATA, PH.D.,‡ HISASHI MORI, PH.D.,§ HIROSHI INOUE, M.D., PH.D.,† YUKIKO HATA, PH.D.,* KENKICHI FUKUROTANI, PH.D.,‡ and NAOKI NISHIDA, M.D., PH.D.*

From the *Department of Legal Medicine; †Second Department of Internal Medicine, Graduate School of Medical and Pharmaceutical Sciences, University of Toyama, Toyama, Japan; ‡Laboratory for Neural Information Technology, Graduate School of Sciences and Engineering, University of Toyama, Toyama, Japan; and §Department of Molecular Neurosciences, Graduate School of Medical and Pharmaceutical Sciences, University of Toyama, Toyama, Japan

**hERG(G487R) Channel.** ***Introduction:*** **Mutations of human *ether-à-go-go*-related gene (hERG), which encodes a cardiac $K^+$ channel responsible for the acceleration of the repolarizing phase of an action potential and the prevention of premature action potential regeneration, often cause severe arrhythmic disorders. We found a novel missense mutation of hERG that results in a G487R substitution in the S2–S3 loop of the channel subunit [hERG(G487R)] from a family and determined whether this mutant gene could induce an abnormality in channel function.**

***Methods and Results:*** **We made whole-cell voltage-clamp recordings from HEK-293T cells transfected with wild-type hERG [hERG(WT)], hERG(G487R), or both. We measured hERG channel-mediated current as the "tail" of a depolarization-elicited current. The current density of the tail current and its voltage- and time-dependences were not different among all the cell groups. The time-courses of deactivation, inactivation, and recovery from inactivation and their voltage-dependences were not different among all the cell groups. Furthermore, we performed immunocytochemical analysis using an anti-hERG subunit antibody. The ratio of the immunoreactivity of the plasma membrane to that of the cytoplasm was not different between cells transfected with hERG(WT), hERG(G487R), or both.**

***Conclusion:*** **hERG(G487R) can produce functional channels with normal gating kinetics and cell-surface expression efficiency with or without the aid of hERG(WT). Therefore, neither the heterozygous nor homozygous inheritance of hERG(G487R) is thought to cause severe cardiac disorders. hERG(G487R) would be a candidate for a rare variant or polymorphism of hERG with an amino acid substitution in the unusual region of the channel subunit.** *(J Cardiovasc Electrophysiol, Vol. 23, pp. 1246-1253, November 2012)*

*arrhythmia, HEK-293T cell, hERG(G487R), KCNH2, $K_v11.1$, patch-clamp, sudden death*

## Introduction

Human *ether-à-go-go*-related gene (hERG) encodes the alpha subunit of a slowly activating, fast inactivating voltage-gated $K^+$ channel expressed in cardiac cells.[1-4] hERG channel undergoes activation as well as inactivation at the early phase of an action potential, producing only a small conductance. hERG channel recovers from inactivation at the repolarizing phase of an action potential[1,2,5] and produces a large conductance at this phase. In turn, this large conductance accelerates repolarization and prevents premature action potential regeneration.[1,2] Mutations of hERG may cause type-2 long-QT syndrome (LQT2), which is characterized by an abnormally long interval between the Q and T waves of the electrocardiogram.[1,2,5-7] LQT2 patients are at risk for severe arrhythmic disorders such as torsades de pointes and sudden cardiac death. To elucidate the structure-function relation of hERG channel and the pathogenic mechanism of LQT2, it is important to analyze the genotype and phenotype of individual mutant hERGs.

Here we report a novel missense mutation of hERG found in the genetic screening of a family (see Results for details). We termed this mutant gene hERG(G487R) because it should produce hERG subunit with a G487R substitution in the S2–S3 loop. A young adult member of this family heterozygously carries hERG(G487R) but has not yet shown any major cardiac disorders. However, it could be possible that the heterozygous inheritance of hERG(G487R) causes major disorders at the late stage of life and/or that the homozygous inheritance of hERG(G487R) does so at an earlier stage. To assess these possibilities, we performed electrophysiological and immunocytochemical analyses of hERG(G487R) products in heterologous expression cells.

¶Y.Y. and K.N. equally contributed to this work.

This work was partly supported by a KAKENHI grant from MEXT, Japan, to Dr. Tabata (#23500384).

No disclosures.

Address for correspondence: Toshihide Tabata, M.S., PH.D., Laboratory for Neural Information Technology, Graduate School of Sciences and Engineering, University of Toyama, 3190 Gofuku, Toyama, Toyama 930-8555, Japan. Fax: 81-76-445-6703; E-mail: ttabata@eng.u-toyama.ac.jp

Manuscript received 13 January 2012; Revised manuscript received 20 March 2012; Accepted for publication 25 April 2012.

doi: 10.1111/j.1540-8167.2012.02383.x

## Methods

### *Genetic Analysis*

The diagnosis of and peripheral blood sampling from the subject family were performed at the Department of Cardiovascular Internal Medicine, Toyama University Hospital (Toyama, Japan) under the approval of the university's committee on utilization of human genes (#22–9). The genomic DNA was extracted from the samples with a QIAamp DNA Mini Kit (Qiagen, Hilden, North Rhine-Westphalia, Germany). The exons 1–15 of hERG were amplified by polymerase chain reaction with intron-flanking primers and purified with a QIAEX II Gel Extraction Kit (Qiagen). DNA sequencing was performed using a PRISM 3100 genetic analyzer (Life Technologies, Carlsbad, CA, USA).

### *Plasmid Construction*

pCAGGS-hERG(WT) vector was generated by inserting hERG(WT) cDNA (NM_000238.3, kindly gifted by Dr. K. Hayashi and Dr. S. Kupershmidt) into the pCAGGS mammalian expression plasmid vector (kindly gifted by Dr. J. Miyazaki)[8] at the *Xho* I-digested site. pCAGGS-hERG(G487R) vector was generated by site-directed mutagenesis on the pCAGGS-hERG(WT) vector.

### *Cell Preparation*

HEK-293T cells were cultured in 10% fetal bovine serum-supplemented Dulbecco's modified Eagle medium (11995–065, Life Technologies) at 37 °C in 5% $CO_2$. Three days before the electrophysiological measurement, the cells were transferred to 35-mm dishes (353001, Becton Dickinson, Franklin Lakes, NJ, USA). Two days before the measurement, the cells were transfected with the pCAGGS-hERG(WT) vector (225 ng/dish), the pCAGGS-hERG(G487R) vector (225 ng/dish), or a 1:1 mixture of these vectors (for each vector, 112.5 ng/dish) and enhanced green fluorescent protein (EGFP) gene-containing pCAGGS vector (25 ng/dish) (WT, GR, and GR/WT cells, respectively) using TransIT-293 reagent (Mirus Bio, Madison, WI, USA).

For immunostaining, HEK-293T cells were cultured on 35-mm glass-base dishes (3911–035, AGC Techno Glass, Funabashi, Chiba, Japan). Two days before immunostaining, the cells were transfected with pCAGGS-hERG(WT) vector (250 ng/dish), pCAGGS-hERG(G487R) vector (250 ng/dish), or a 1:1 mixture of these vectors (for each vector, 125 ng/dish) using TransIT-293 reagent. For negative control, cells were incubated with the reagent alone.

### *Electrophysiological Analysis*

Rupture-patch whole-cell voltage-clamp recordings were made from the EGFP-positive cells. A glass recording pipette (tip resistance, ~5 MΩ) was filled with a pipette solution containing (in mM) 134 potassium D-gluconic acid, 7.6 KCl, 9 KOH, 10 NaCl, 1.2 $MgCl_2$, 10 HEPES, 0.5 EGTA, and 4 adenosine triphosphate magnesium salt (pH, adjusted to 7.3 with KOH; total $K^+$ concentration, ~153 mM). The recording chamber (i.e., culture dish) was perfused at a rate of 1.2 mL/min with a prewarmed (36–38 °C) bath solution containing (in mM) 147 NaCl, 3 KCl, 2 $CaCl_2$, 1 $MgCl_2$, 10 HEPES, and 10 D-glucose (pH, adjusted to 7.4 with NaOH; total $Na^+$ concentration, ~153 mM).

The command voltages were corrected for a liquid junction potential between the pipette and bath solutions. Current signals were acquired with an EPC 8 amplifier (HEKA, Lambrecht, Rhineland-Palatinate, Germany; cut-off frequency, 5 kHz; sampling frequency, 20 or 50 kHz) controlled by PatchMaster software (version, 2×35; HEKA). The holding potential was –80 mV. After a recording configuration was established, the pipette capacitance was canceled electronically and responses to 10 sets of bipolar voltage pulses (+5 mV for 40 milliseconds and –5 mV for 40 milliseconds) were recorded. Then, the main component of the membrane capacitance ($C_m$) was canceled electronically and responses were recorded with 60% electronic series resistance compensation. In the experiments on inactivation and recovery from inactivation, on-line linear leakage subtraction was performed with 5 sets of 0.1-scaled command voltage steps.

In the experiment shown in Figure 2A–C, the current traces were low-pass-filtered at a cut-off frequency of 150 Hz off-line using IGOR Pro software (version, 6.22A; WaveMetrics, Portland, OR, USA) and then used for amplitude analysis. The cell membrane conductance and $C_m$ were estimated from the average of the pulse-evoked responses and used for off-line linear leakage subtraction and current density calculation (Fig. 2). To quantify the voltage-dependence of activation extent, a Boltzmann equation [$I_{hERG} = A/(1 + (V_{half} - V_{comm}) / K)$, where $I_{hERG}$, A, $V_{half}$, $V_{comm}$, and K are the amplitude of hERG channel current, scale factor, voltage for half-maximal activation, command potential, and slope, respectively] was fitted to the plot of normalized peak tail current amplitude against first-step voltage (*cf.* Fig. 2C) of each cell using IGOR Pro software. For this fitting, the data of amplitudes in a first-step voltage range from –40 mV to 20 mV higher than the maximal-activation voltage were collected from the cells tested with a second-step voltage of –40 mV (Fig. 2A, C); the amplitudes at first-step voltages of –60 and –50 mV were taken as 0 because they were negligible in the WT, GR, and GR/WT cells (Fig. 2C). To quantify the time-dependence of gating, a single- or double-exponential curve was fitted to the rising or decaying phase of the current trace using IGOR Pro software. Each numerical data group is expressed as mean ± SEM throughout the text, table, and figures. Unpaired *t*-test was used to examine statistical differences between data groups when the majority of the groups had normal distributions ($P > 0.05$, Shapiro–Wilk test). Median or Wilcoxon rank sum test was used when the data groups had Gumbel-like and quasi-normal distributions, respectively.

### *Immunostaining*

The cells were treated consecutively with Dulbecco's phosphate buffers containing the following reagents: 4% paraformaldehyde (room temperature [RT], 20 minutes), 0.2% Triton X-100 (28314, Thermo Fisher Scientific, Rockford, IL, USA; RT, 5 minutes), Image-iT FX signal enhancer (I36933, Life Technologies; RT, 30 minutes), a rabbit anti-hERG channel subunit primary antibody (APC-190, Alomone, Jerusalem, Israel; 1:100) and 1% bovine serum albumin fraction V (4 °C, overnight), and Alexa 647-conjugated goat anti-rabbit IgG(H+L) secondary antibody (A21245, Life Technologies; 1:250, 37 °C, 60 minutes).

For moderately stained cells, single image slices of He/Ne laser beam-excited immunofluorescence were captured using

a TCS-SC5 confocal microscope (Leica, Solms, Hesse, Germany; objective lens, water- or oil-immersion, x63; pinhole, airy 1; window, 655–685 nm; gain, 700–740 V; scanning rate, 200 Hz; number of averaging, 16). In each image slice, raw fluorescent intensities were measured as averages over a 1.3-$\mu m^2$ strip area on the membrane and a 4-$\mu m^2$ rectangular area in the cytoplasm using ImageJ software (version, 1.45S; National Institutes of Health, Bethesda, MD, USA). The intensity was corrected for the background level by subtracting the average intensity over four 17-$\mu m^2$ cell-free square areas of the corresponding image slice from the raw value.

## Results

### *Genetic Analysis*

In the family genetic screening of sudden cardiac death victims, we found a Japanese family with members heterozygously carrying hERG(G487R) and/or a mutant SCN5A gene encoding a voltage-gated $Na^+$ channel subunit with a R1193Q substitution (SCN5A(R1193Q), see Discussion for detail; Fig. 1A). A male member of this family carrying SCN5A(R1193Q) but not hERG(G487R) died from sudden cardiac death at the age of 19. By contrast, his sister carrying hERG(G487R) but not SCN5A(R1193Q) has not yet shown any major cardiac symptoms up to the same age. All the members displayed normal Bazzett-corrected QT intervals (QTc's; Fig. 1A) and turned out to carry no missense mutations in other major long-QT syndrome-related voltage-gated ion channel genes including KCNE1, KCNE2, and KCNQ1.

We found a G1459C replacement in hERG from the family (Fig. 1B). This replacement should result in a G487R substitution in the S2–S3 loop of hERG channel subunit (Fig. 1C). The amino acid sequence of the S2–S3 loop is conserved among the mammalian homologs (human, NP_000229.1; chimpanzee, XP_001137384.2; rabbit, NP_001075853.1; mouse, NP_038597.2; pig, Q9TUI4; horse, NP_001180587.1; dog, NP_001003145; Fig. 1D).

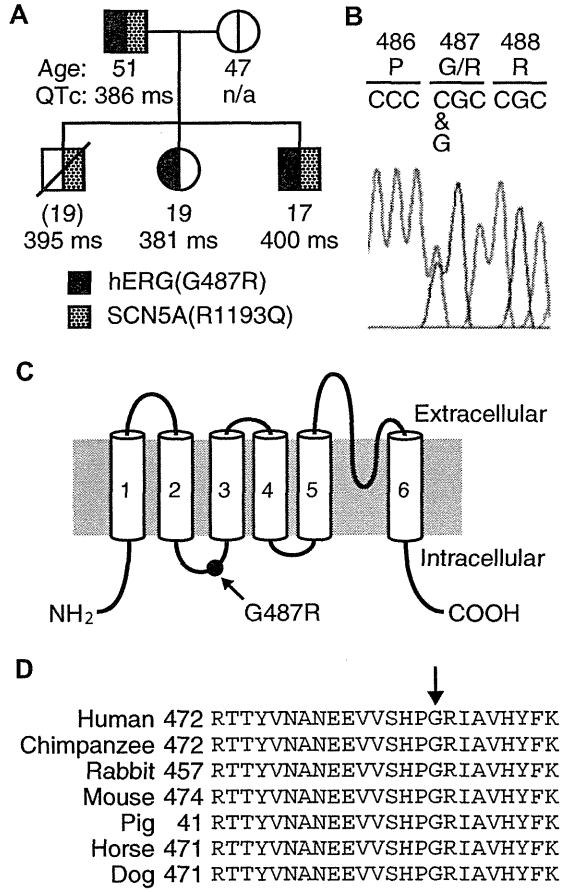


**Figure 1.** *Mutation causing a G487R substitution of hERG channel subunit. A: Pedigree of the subject family. Most members heterozygously carry hERG(G487R) (black rectangle) and/or SCN5A(R1193Q) (dotted rectangle). The age and values of QTc are shown below the corresponding symbols (n/a: not available). Slash: the person deceased from sudden cardiac death at the age of 19. Squares and circles: male and female members, respectively. B: DNA sequencing profile of the exon 5 of hERG from the hERG(G487R)-carrying female member of the subject family. The amino acids encoded by the codons are indicated above the sequence. C: Schematic diagram showing the location of the G487R substitution in hERG channel subunit. D: Amino acid sequences of the S2–S3 loops of hERG(WT) subunit and the mammalian homologs. Number before the sequence: the position of the first residue of the loop. Arrow: the site of the G487R substitution.*

### *Electrophysiological Analysis*

We compared currents in the WT, GR, and GR/WT cells, which are thought to be mediated largely by homomeric hERG(WT), homomeric hERG(G487R), and heteromeric hERG(G487R)/hERG(WT) channels, respectively. The activation and deactivation kinetics of hERG channels were analyzed using a double-voltage-step stimulus (Fig. 2). At the first step whose voltage was relatively high, hERG channel underwent activation as well as inactivation. At the second step whose voltage was less positive, hERG channel was allowed to recover from inactivation and produced a large "tail" current (Fig. 2A, arrows). The tail current measured under the conditions used in this study included virtually no component mediated by HEK-293T cell's native voltage-dependent channel because the native current decayed rapidly upon the cessation of the first step (Fig. 2A) and its current density at the second voltage step was negligible (with a first-step voltage of 0 mV, 0.579 ± 0.482 pA/pF, n = 7; P = 0.0027 compared with the WT cells, median test; Fig. 2B).

We used the peak density of the tail current as a measure of the activation extent of hERG channel (Fig. 2B). In all the cell groups, hERG channels were activated with first-step voltages above ~–40 mV. The activation extent increased with first-step voltage until it became saturated with first-step voltages above 0 mV. With a first-step voltage of 0 mV, the current densities were 164 ± 18.1 pA/pF (n = 21), 162 ± 19.9 pA/pF (n = 18), and 198 ± 17.5 pA/pF (n = 33) for the WT, GR, and GR/WT cells, respectively. There was no significant difference between the WT and GR cells or between the WT and GR/WT cells (P = 0.435 and 0.407, respectively, median test). Moreover, the plot of the relative peak amplitude of the tail current against first-step voltage was indistinguishable between the WT, GR, and GR/WT cells (Fig. 2C). The $V_{half}$ and K were not different between these cell groups (Table 1). These results suggest that hERG(G487R) subunit-containing hERG channels are similar to hERG(WT) channel in activation extent and its voltage dependence.

The activation time-course of hERG channel was demonstrated by varying the first-step duration and by plotting the relative peak amplitude of the tail current against the duration (Fig. 2D). The time constant of the rising phase of the plot

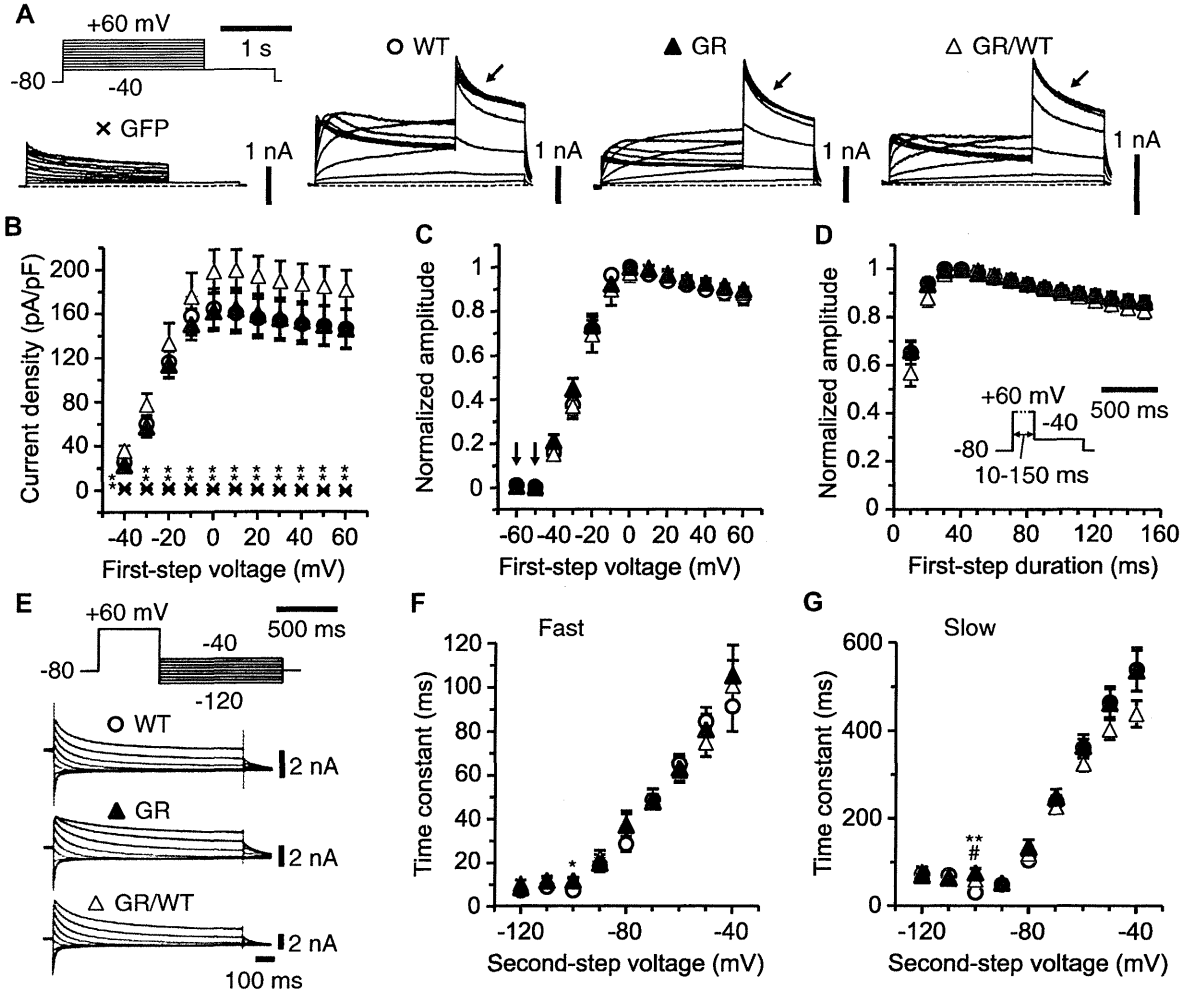


**Figure 2.** *Activation and deactivation kinetics. A–C: Activation extent of hERG channels and its voltage-dependence. A: Sample responses of individual cells (traces) to double-voltage-step stimuli (schematics). The first-step voltage was varied in 10 mV steps. GFP: a cell transfected with the marker gene alone. WT, GR, and GR/WT: cells transfected with hERG(WT), hERG(G487R), or a 1:1 mixture of these genes, respectively. The "tail" currents (arrows) are thought to be mediated largely by hERG channels because no similar current is seen in the GFP cell. The traces include linear leak components. Dotted line: prestimulus level. B: Mean peak density of the tail current as a function of first-step voltage. As compared with the current density of the WT cells, that of the GFP cells was significantly different at all of the tested voltages ($P < 0.01$, median test;**) whereas those of the GR and GR/WT cells were not different ($P > 0.05$, median test) at all of the tested voltages. The data were taken from 7 GFP, 21 WT, 18 GR, and 33 GR/WT cells. The peak amplitude was measured as a difference from the average level of the 100 millisecond prestimulus period to the maximal deflection throughout the second voltage step. In panels B–D, the linear leak components were subtracted from the data off-line. C: Relative peak amplitude of the tail current as a function of first-step voltage. To depict the plots in this panel, the data in panel B were maximum-normalized for each cell and then averaged and maximum-normalized within each cell group. The data plotted against first-step voltages of –60 and –50 mV (arrows) were obtained using double-voltage-step stimuli whose second-step voltage was –60 mV. D: Activation time-course of hERG channels. Mean relative peak amplitude of the tail current elicited by a double-voltage-step stimulus plotted as a function of first-step duration. The duration was varied as shown schematically in the inset. The data were maximum-normalized for each cell and then averaged and maximum-normalized within each cell group. The data were taken from 16 WT, 20 GR, and 19 GR/WT cells. E–G: Deactivation time-course of hERG channels and its voltage dependence. E: Sample tail currents of individual cells (close-up traces around the second voltage step) elicited by double-voltage-step stimuli (schematics). The second-step voltage was varied in 10 mV steps. F and G: Mean time constants of the fast (F) and slow (G) components of deactivation as functions of second-step voltage. The data were taken from 14 WT, 16 GR, and 25 GR/WT cells.* and**: $P < 0.05$ (Wilcoxon test) and $P < 0.01$ (t-test) between the WT and GR cells, respectively. #: $P < 0.05$ (Wilcoxon test) between the WT and GR/WT cells. The time constants were estimated from the double-exponential curve fitted to the decaying phase of a tail current.*

was not different between the WT and GR cells or between the WT and GR/WT cells (Table 1). This result suggests that hERG(G487R) subunit-containing hERG channels are similar to hERG(WT) channel in activation time-course.

The deactivation kinetics of hERG channels was analyzed, measuring the time constant of the decaying phase of the tail current with a varied second-step voltage (Fig. 2E). The time constants of both the fast and slow components of the decaying phase decreased with more negative second-step voltages. The time constants of both the fast and slow components were not different between the cell groups at most of the tested voltages (Fig. 2F and G). At a second-step voltage of –40 mV, the time constants of the fast and slow components were 0.0912 ± 0.0114 milliseconds (n = 13) and 0.539 ± 0.0492 milliseconds (n = 13), 0.105 ± 0.0138 milliseconds (n = 15) and 0.537 ± 0.0454 milliseconds (n = 16), and 0.101 ± 0.0114 milliseconds (n = 25) and 0.439 ± 0.0303 milliseconds (n = 25) for the WT, GR, and

**TABLE 1**
Parameters of Activation Kinetics

| Cell | $V_{half}$ (mV) | K | Time Constant (ms) |
|---|---|---|---|
| WT | −27.3 ± 1.38 (19, n/a) | 5.42 ± 0.207 (19, n/a) | 9.31 ± 1.58 (16, n/a) |
| GR | −25.1 ± 2.53 (17, 0.449) | 5.18 ± 0.127 (17, 0.514) | 9.52 ± 1.07 (20, 0.924) |
| GR/WT | −27.9 ± 1.75 (29, 0.831) | 5.42 ± 0.260 (29, 0.999) | 12.9 ± 1.97 (19, 0.121) |

The $V_{half}$ and K were estimated from the Boltzmann equation fitted to the plot of activation extent against first-step voltage (*cf.* Fig. 2C) for each cell. The time constant was estimated from the single-exponential curve fitted to the rising period (a range of first-step duration from 0 to the point at which the activation extent became saturated) of the plot of activation extent against first-step duration (*cf.* Fig. 2D) for each cell. Numbers in parentheses = the number of the examined cells and the significance level of difference (as compared with the WT cells, *t*-test); n/a = not applicable.

GR/WT cells, respectively. There was no significant difference between the WT and GR cells or between the WT and GR/WT cells (for the fast component, P = 0.447 and 0.724, respectively, Wilcoxon test; for the slow component, P = 0.973 and 0.0859, respectively, *t*-test). This result suggests that hERG(G487R) subunit-containing hERG channels are similar to hERG(WT) channel in deactivation time-course and its voltage dependence.

The inactivation kinetics of hERG channels was analyzed using a triple-voltage-step stimulus (Fig. 3A). The hERG channel that had undergone activation and inactivation was allowed to recover from inactivation at the second hyperpolarizing step and then again inactivated at the third step of a varied voltage. The time constant of the decaying phase of the tail current decreased with more positive third-step voltages (Fig. 3B). At a third-step voltage of 40 mV, the time constants were 0.632 ± 0.0267 milliseconds (n = 15), 0.607 ± 0.0634 milliseconds (n = 14), and 0.662 ± 0.0536 milliseconds (n = 14) for the WT, GR, and GR/WT cells, respectively. There was no significant difference between the WT and GR cells or between the WT and GR/WT cells (P = 0.723 and 0.661, respectively, *t*-test). This result suggests that hERG(G487R) subunit-containing channels are similar to hERG(WT) channel in inactivation time-course and its voltage dependence.

The kinetics of the recovery from inactivation of hERG channels was analyzed using a double-voltage-step stimulus (Fig. 3C). The hERG channel that had undergone activation and inactivation at the first depolarizing step was allowed to recover from inactivation at the second step of a more negative voltage. The time constant of the rising phase of the tail current decreased with more negative second-step voltages (Fig. 3D). At a second-step voltage of −40 mV, the time constants were 2.07 ± 0.120 milliseconds (n = 14), 1.88 ± 0.119 milliseconds (n = 10), and 2.20 ± 0.139 milliseconds (n = 13) for the WT, GR, and GR/WT cells, respectively. There was no significant difference between the WT and GR cells or between the WT and GR/WT cells (P = 0.327 and 0.440, respectively, *t*-test). This result suggests that hERG(G487R) subunit-containing channels are similar to hERG(WT) channel in the time-course of recovery from inactivation and its voltage dependence.

### *Immunocytochemical Analysis*

We examined the subcellular distribution of hERG(WT) and hERG(G487R) channel subunits in HEK-293T cells using an anti-hERG subunit antibody. All of the cultures transfected with hERG(WT), hERG(G487R), or a 1:1 mixture of these genes contained cells with an intense immunoreactivity on the membrane and a weaker immunoreactivity in the cytoplasm (Fig. 4A). Cells receiving mock transfection (mock cells) showed no such immunoreactivity (Fig. 4A), suggesting the correct recognition of the antigen. The ratios of the immunofluorescent signal intensity of the membrane to that of the cytoplasm were 2.41 ± 0.213 (n = 20), 2.32 ± 0.156 (n = 24), and 2.87 ± 0.293 (n = 12) for the WT, GR, and GR/WT cells, respectively (Fig. 4B). There was no significant difference between the WT and GR cells (P = 0.710, *t*-test) or between the WT and GR/WT cells (P = 0.205, *t*-test). This result suggests that hERG(G487R) subunit can be trafficked to the cell surface as efficiently as hERG(WT) subunit and that the coexpression of these subunits does not suppress the total channel trafficking. The ratios of the gene-transfected cells were much different from that of the mock cells (0.195 ± 0.0918, n = 5; P < 0.001 compared with the WT cells, *t*-test), suggesting that these ratios of the gene-transfected cells indeed reflect the subcellular distributions of hERG subunits. The mock cells showed a ratio lower than 1 (i.e., the fluorescent signal of the membrane is weaker than that of the cytoplasm) presumably because most of the antibodies that had attached to the cell surface were washed off whereas a small fraction of the antibodies that had entered the cells remained in the cytoplasm in a nonspecific manner (Fig. 4A).

## Discussion

The density of hERG channel current (Fig. 2B) and the surface expression efficiency of hERG subunit (Fig. 4) were not different between the WT and GR cells. These results suggest that hERG(G487R) subunit can form functional channels as efficiently as hERG(WT) subunit. Moreover, there was no difference in the current density (Fig. 2B) or surface expression efficiency (Fig. 4) between the WT and GR/WT cells. This result suggests that hERG(G487R) subunit does not serve as a dominant negative that hampers the formation of functional WT subunit-containing channels.

The voltage- and time-dependences of activation, deactivation, inactivation, and recovery from inactivation of hERG channel current were similar between the WT, GR, and GR/WT cells (Figs. 2 and 3). These results suggest that hERG(G487R) subunit-containing channels can contribute to the acceleration of the repolarizing phase of a cardiac action potential and to the prevention of premature action potential regeneration.[1,2] The normal gating kinetics and normal functional expression efficiency (see earlier) of hERG(G487R) subunit-containing channels indicate that neither the heterozygous nor homozygous inheritance of hERG(G487R) may cause severe cardiac disorders.

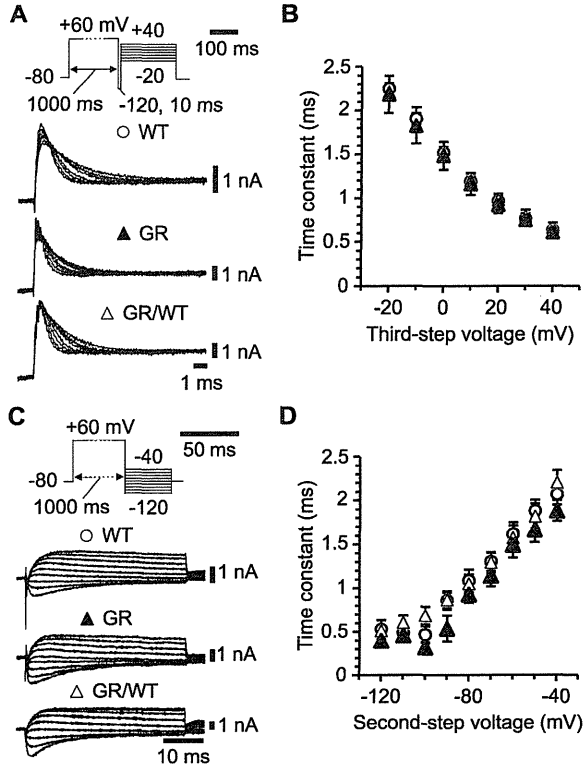


**Figure 3.** *Kinetics of inactivation and recovery from inactivation. A and B: Inactivation time-course of hERG channels and its voltage dependence. A: Sample current responses (close-up traces around the third step) of individual cells to triple-voltage-step stimuli (schematics). hERG channel was allowed to recover from inactivation at the second hyperpolarizing step and then again inactivated at the third step whose voltage was varied in 10 mV steps. B: Mean time constant of inactivation as a function of third-step voltage. The data were taken from 15 WT, 14 GR, and 14 GR/WT cells. There was no significant difference (P > 0.05, t-test) between the WT and GR cells or between the WT and GR/WT cells at all the tested voltages. The time constant was estimated from the single-exponential curve fitted to an inactivating current at the third step. C and D: Time-course of the recovery from inactivation of hERG channels and its voltage dependence. C: Sample current responses (close-up around the second step) of individual cells to double-voltage-step stimuli (schematics). hERG channel was inactivated at the first depolarizing step and then allowed to recover from inactivation at the onset of the second step whose voltage was varied in 10 mV steps. D: Mean time constant of recovery from inactivation as a function of second-step voltage. The data were taken from 14 WT, 10 GR, and 13 GR/WT cells. There was no significant difference (P > 0.05, t-test) between the WT and GR cells or between the WT and GR/WT cells at all the tested voltages. The time constant was estimated from the single-exponential curve fitted to the initial rise of a current at the second step.*

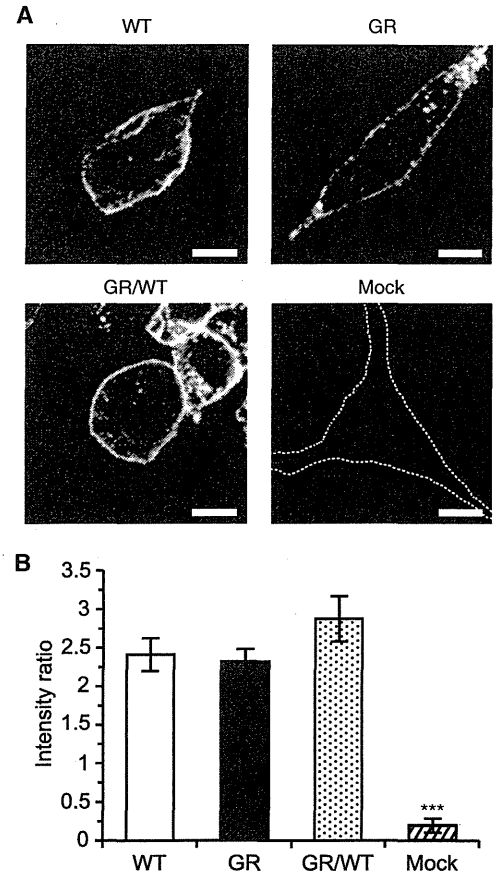


**Figure 4.** *Subcellular distribution of hERG channel subunits. A and B: Immunostaining of HEK-293T cells transfected with hERG(WT), hERG(G487R), or a 1:1 mixture of these genes (WT, GR, and GR/WT, respectively). A: Single confocal image slices of cells stained using the anti-hERG subunit antibody. Mock: a cell treated with the transfection reagent alone without hERG(WT) or hERG(G487R) (the outline of the cell is indicated by dotted lines). Scale bars: 10 μm. B: Mean ratio of the immunofluorescent signal intensity of the membrane to that of the cytoplasm. The data were taken from 20 WT, 24 GR, 12 GR/WT, and 5 mock cells. As compared with the ratio of the WT cells, those of the GR and GR/WT cells were not significantly different (P > 0.05, t-test) whereas that of the mock cells was significantly different (P < 0.001, t-test;***).*

In the subject family, a member carrying SCN5A (R1193Q) but not hERG(G487R) died from sudden cardiac death (Fig. 1A). By contrast, his father carrying both hERG(G487R) and SCN5A(R1193Q) is still living without showing major cardiac symptoms (Fig. 1A). This variability in cardiac phenotype might reflect the low phenotypic penetrance of SCN5A(R1193Q). There are some reports suggesting the linkage of SCN5A(R1193Q) to QT and Brugada syndromes.[9,10] However, in some Asian cohorts, comparable allelic frequencies of SCN5A(R1193Q) are found in both the arrhythmic patients and the healthy persons.[11,12] Another possible explanation is that hERG(G487R) have a protective effect against the pathogenic action of SCN5A(R1193Q) whereas this might not be the case because hERG(G487R) subunit-containing channels were functionally similar to homomeric hERG(WT) channel (Figs. 2 and 3).

It could be theoretically possible that on a global scale, a considerable fraction of the population carry hERG(G487R) because hERG(G487R) was inherited across generations (Fig. 1A) and its product did not change channel function (Figs. 2 and 3). For hERG, some examples of amino acid polymorphism such as K897T, A915V, and R1047L have been reported.[13-15] However, to our knowledge, hERG(G487R) has not been reported previously and, thus, this mutant gene might fall into the category of a rare variant. One possibility is that hERG(G487R) emerged through *de novo* mutation in the subject family or their immediate ancestor. We do not exclude the possibility that hERG(G487R) is common in an uninvestigated ethnic or regional cohort as suggested by a wide intercohort deviation in the allelic frequencies of the previously reported amino acid polymorphisms.[13-19]

The amino acid substitution examined in this study is located in the S2–S3 loop (Fig. 1C). The previous and present reports show that several amino acid changes in and near this loop result in various channel phenotypes. For example, the N470D substitution impairs the surface expression of the channel protein[20] and lowers the $V_{half}$.[21] The T474I substitution lowers the threshold and maximal-activation voltages and hERG subunit with this substitution suppresses channel current in a dominant-negative manner.[22,23] The Y475 deletion lowers the $V_{half}$ and accelerates the deactivation.[21] The A490T substitution reduces the current density.[24] Furthermore, we have shown that the G487R substitution causes none of these abnormalities (Figs. 2-4). These findings are in contrast to the report that several substitutions at different amino acid residues in the S5/pore domain (G572R, I593R, P596R, G601S, Y611H, V612L, and T613M) similarly impair channel protein trafficking (see Ref. 25 for review). The individual residues in and near the S2–S3 loop may play distinct physiological and pathogenic roles in a relatively highly site-specific manner as compared to the residues in other regions.

The previous studies indicate that the extent of functional modulation of hERG channel induced by a substitution at a glycine residue depends on the position of the residue. For example, the substitution of glycine in the S4–S5 linker (G546) with another amino acid such as alanine or arginine markedly lowers the $V_{half}$.[26] This could be ascribed to loss of the conformational flexibility of the linker conferred by the glycine residue.[26] By contrast, alanine substitutions of glycine residues in the S6 (G648 and G657), which could increase the local conformational stability, have only a minor effect on the voltage dependence of activation.[27] One possible explanation is that the S6 helices are inherently flexible even in the absence of the glycine residues.[27] Our observation that the G487R substitution little affected the gating kinetics (Figs. 2 and 3) indicates that the flexibility conferred by the glycine residue might be less important for the normal function of the S2–S3 loop.

## Conclusion

We found a novel mutation of hERG that results in a G487R substitution in the S2–S3 loop of hERG channel. In HEK-293T cells, hERG with this mutation produced functional channels with or without the aid of wild-type hERG. Both the heteromeric and homomeric mutant hERG channels displayed similar kinetics of activation, deactivation, inactivation, and recovery from inactivation to wild-type channel. These results indicate that neither the heterozygous nor homozygous inheritance of the mutant hERG may cause severe cardiac disorders.

*Acknowledgments:* We thank the providers of the gene samples for their kind cooperation. We thank Y. Fujita, M.S., and T. Shimomura, M.S., for their pilot study.

## References

1. Perrin MJ, Subbiah RN, Vandenberg JI, Hill AP: Human ether-a-go-go related gene (hERG) $K^+$ channels: Function and dysfunction. Prog Biophys Mol Biol 2008;98:137-148.
2. Sanguinetti MC, Tristani-Firouzi M: hERG potassium channels and cardiac arrhythmia. Nature 2006;440:463-469.
3. Trudeau MC, Warmke JW, Ganetzky B, Robertson GA: HERG, a human inward rectifier in the voltage-gated potassium channel family. Science 1995;269:92-95.
4. Warmke JW, Ganetzky B: A family of potassium channel genes related to *eag* in *Drosophila* and mammals. Proc Natl Acad Sci USA 1994;91:3438-3442.
5. Ravens U, Cerbai E: Role of potassium currents in cardiac arrhythmias. Europace 2008;10:1133-1137.
6. Keating MT, Sanguinetti MC: Molecular and cellular mechanisms of cardiac arrhythmias. Cell 2001;104:569-580.
7. Splawski I, Shen J, Timothy KW, Lehmann MH, Priori S, Robinson JL, Moss AJ, Schwartz PJ, Towbin JA, Vincent GM, Keating MT: Spectrum of mutations in long-QT syndrome genes. *KVLQT1*, *HERG*, *SCN5A*, *KCNE1*, and *KCNE2*. Circulation 2000;102:1178-1185.
8. Niwa H, Yamamura K, Miyazaki J: Efficient selection for high-expression transfectants with a novel eukaryotic vector. Gene 1991;108:193-199.
9. Wang Q, Chen S, Chen Q, Wan X, Shen J, Hoeltge GA, Timur AA, Keating MT, Kirsch GE: The common *SCN5A* mutation R1193Q causes LQTS-type electrophysiological alterations of the cardiac sodium channel. J Med Genet 2004;41:e66.
10. Huang H, Zhao J, Barrane FZ, Champagne J, Chahine M: $Na_v1.5$/R1193Q polymorphism is associated with both long QT and Brugada syndromes. Can J Cardiol 2006;22:309-313.
11. Ackerman MJ, Splawski I, Makielski JC, Tester DJ, Will ML, Timothy KW, Keating MT, Jones G, Chadha M, Burrow CR, Stephens JC, Xu C, Judson R, Curran ME: Spectrum and prevalence of cardiac sodium channel variants among black, white, Asian, and Hispanic individuals: Implications for arrhythmogenic susceptibility and Brugada/long QT syndrome genetic testing. Heart Rhythm 2004;1:600-607.
12. Maekawa K, Saito Y, Ozawa S, Adachi-Akahane S, Kawamoto M, Komamura K, Shimizu W, Ueno K, Kamakura S, Kamatani N, Kitakaze M, Sawada J: Genetic polymorphisms and haplotypes of the human cardiac sodium channel alpha subunit gene (*SCN5A*) in Japanese and their association with arrhythmia. Ann Hum Genet 2005;69:413-428.
13. Ackerman MJ, Tester DJ, Jones GS, Will ML, Burrow CR, Curran ME: Ethnic differences in cardiac potassium channel variants: Implications for genetic susceptibility to sudden cardiac death and genetic testing for congenital long QT syndrome. Mayo Clin Proc 2003;78:1479-1487.
14. Laitinen P, Fodstad H, Piippo K, Swan H, Toivonen L, Viitasalo M, Kaprio J, Kontula K: Survey of the coding region of the HERG gene in long QT syndrome reveals six novel mutations and an amino acid polymorphism with possible phenotypic effects. Hum Mutat 2000;15:580-581.
15. Larsen LA, Andersen PS, Kanters J, Svendsen IH, Jacobsen JR, Vuust J, Wettrell G, Tranebjaerg L, Bathen J, Christiansen M: Screening for mutations and polymorphisms in the genes *KCNH2* and *KCNE2* encoding the cardiac HERG/MiRP1 ion channel: Implications for acquired and congenital long Q-T syndrome. Clin Chem 2001;47:1390-1395.
16. Anson BD, Ackerman MJ, Tester DJ, Will ML, Delisle BP, Anderson CL, January CT: Molecular and functional characterization of common polymorphisms in HERG (KCNH2) potassium channels. Am J Physiol Heart Circ Physiol 2004;286:H2434-H2441.
17. Aydin A, Bahring S, Dahm S, Guenther UP, Uhlmann R, Busjahn A, Luft FC: Single nucleotide polymorphism map of five long-QT genes. J Mol Med (Berl) 2005;83:159-165.
18. Koo SH, Ho WF, Lee EJ: Genetic polymorphisms in KCNQ1, HERG, KCNE1 and KCNE2 genes in the Chinese, Malay and Indian populations of Singapore. Br J Clin Pharmacol 2006;61:301-308.
19. Mannikko R, Overend G, Perrey C, Gavaghan CL, Valentin JP, Morten J, Armstrong M, Pollard CE: Pharmacological and electrophysiological characterization of nine, single nucleotide polymorphisms of the hERG-encoded potassium channel. Br J Pharmacol 2010;159:102-114.
20. Gong Q, Anderson CL, January CT, Zhou Z: Pharmacological rescue of trafficking defective HERG channels formed by coassembly of wild-type and long QT mutant N470D subunits. Am J Physiol Heart Circ Physiol 2004;287:H652-H658.
21. Lin EC, Holzem KM, Anson BD, Moungey BM, Balijepalli SY, Tester DJ, Ackerman MJ, Delisle BP, Balijepalli RC, January CT: Properties of WT and mutant hERG $K^+$ channels expressed in neonatal mouse cardiomyocytes. Am J Physiol Heart Circ Physiol 2010;298:H1842-H1849.

22. Nakajima T, Furukawa T, Tanaka T, Katayama Y, Nagai R, Nakamura Y, Hiraoka M: Novel mechanism of HERG current suppression in LQT2: Shift in voltage dependence of HERG inactivation. Circ Res 1998;83:415-422.
23. Zhou Z, Gong Q, Epstein ML, January CT: HERG channel dysfunction in human long QT syndrome. Intracellular transport and functional defects. J Biol Chem 1998;273:21061-21066.
24. Yoshida H, Horie M, Otani H, Kawashima T, Onishi Y, Sasayama S: Bradycardia-induced long QT syndrome caused by a de novo missense mutation in the S2-S3 inner loop of *HERG*. Am J Med Genet 2001;98:348-352.
25. Lian J, Huang N, Zhou J, Ge S, Huang X, Huo J, Liu L, Xu W, Zhang S, Yang X, Zhou J, Huang C: Novel characteristics of a trafficking-defective G572R-hERG channel linked to hereditary long QT syndrome. Can J Caridol 2010;26:417-422.
26. Van Slyke AC, Rezazadeh S, Snopkowski M, Shi P, Allard CR, Claydon TW: Mutation within the S4-S5 linker alter voltage sensor constraints in hERG $K^+$ channels. Biophys J 2010;99:2841-2852.
27. Hardman RM, Stansfeld PJ, Dalibalta S, Sutcliffe MJ, Mitcheson JS: Activation gating of hERG potassium channels: S6 glycines are not required as gating hinges. J Biol Chem 2007;282:31972-31981.

OPEN ACCESS Freely available online

PLoS one

# Role of Serine Racemase in Behavioral Sensitization in Mice after Repeated Administration of Methamphetamine

**Mao Horio[1], Mami Kohno[1], Yuko Fujita[1], Tamaki Ishima[1], Ran Inoue[2], Hisashi Mori[2], Kenji Hashimoto[1]***

**1** Division of Clinical Neuroscience, Chiba University Center for Forensic Mental Health, Chiba, Japan, **2** Department of Molecular Neuroscience, Toyama University Graduate School of Medicine, Toyama, Japan

## Abstract

***Background:*** The *N*-methyl-D-aspartate (NMDA) receptors play a role in behavioral abnormalities observed after administration of the psychostimulant, methamphetamine (METH). Serine racemase (SRR) is an enzyme which synthesizes D-serine, an endogenous co-agonist of NMDA receptors. Using *Srr* knock-out (KO) mice, we investigated the role of SRR on METH-induced behavioral abnormalities in mice.

***Methodology/Principal Findings:*** Evaluations of behavior in acute hyperlocomotion, behavioral sensitization, and conditioned place preference (CPP) were performed. The role of SRR on the release of dopamine (DA) in the nucleus accumbens after administration of METH was examined using *in vivo* microdialysis technique. Additionally, phosphorylation levels of ERK1/2 proteins in the striatum, frontal cortex and hippocampus were examined using Western blot analysis. Acute hyperlocomotion after a single administration of METH (3 mg/kg) was comparable between wild-type (WT) and *Srr*-KO mice. However, repeated administration of METH (3 mg/kg/day, once daily for 5 days) resulted in behavioral sensitization in WT, but not *Srr*-KO mice. Pretreatment with D-serine (900 mg/kg, 30 min prior to each METH treatment) did not affect the development of behavioral sensitization after repeated METH administration. In the CPP paradigm, METH-induced rewarding effects were demonstrable in both WT and *Srr*-KO mice. *In vivo* microdialysis study showed that METH (1 mg/kg)-induced DA release in the nucleus accumbens of *Srr*-KO mice previously treated with METH was significantly lower than that of the WT mice previously treated with METH. Interestingly, a single administration of METH (3 mg/kg) significantly increased the phosphorylation status of ERK1/2 in the striatum of WT, but not *Srr*-KO mice.

***Conclusions/Significance:*** These findings suggest first, that SRR plays a role in the development of behavioral sensitization in mice after repeated administration of METH, and second that phosphorylation of ERK1/2 by METH may contribute to the development of this sensitization as seen in WT but not *Srr*-KO mice.

**Citation:** Horio M, Kohno M, Fujita Y, Ishima T, Inoue R, et al. (2012) Role of Serine Racemase in Behavioral Sensitization in Mice after Repeated Administration of Methamphetamine. PLoS ONE 7(4): e35494. doi:10.1371/journal.pone.0035494

**Editor:** Bernard Le Foll, Centre for Addiction and Mental Health, Canada

**Received** February 15, 2012; **Accepted** March 20, 2012; **Published** April 18, 2012



**Funding:** This study was supported by grants from Grants-in-Aid for Scientific Research of Japan Society for the Promotion of Science, Japan (to K.H.) and Intramural Research Grant for Neurological and Psychiatric Disorders of National Center of Neurology and Psychiatry (NCNP), Japan (to K.H.). The funders had no role in study design, data collection and analysis, decision to publish, or preparation of the manuscript.

**Competing Interests:** The authors have declared that no competing interests exist.

* E-mail: hashimoto@faculty.chiba-u.jp

## Introduction

Abuse of the psychostimulant methamphetamine (METH) is a serious and growing worldwide problem. Long-term use of METH results in addiction, which is characterized by compulsive drug-seeking and drug use, with accompanying functional and molecular changes in the brain. Addiction to METH is also a major public health concern, since chronic use is associated with major medical, psychiatric, cognitive, socioeconomic and legal consequence [1,2]. Repeated consumption of METH can induce a psychotic state (METH psychosis), with symptoms resembling those of paranoid-type schizophrenia [3–5]. There is currently no standard pharmacological treatment for the wide range of symptoms associated with METH abuse [1,6,7]. Moreover, the precise molecular and cellular mechanisms underlying the long-term effects of METH in the brain, remain undetermined [1,8,9].

METH causes neurochemical changes in several areas of the brain via the dopaminergic system, and consequently via glutamatergic neurotransmission [10–13]. Repeated administration of this psychostimulant to rodents, produces long-term behavioral changes, including behavioral sensitization and dependence [14,15]. The *N*-methyl-D-aspartate (NMDA) receptor antagonist MK-801 blocks the development of METH (or amphetamine)-induced behavioral sensitization [16–20]. It is therefore likely that the NMDA receptor plays a role in the mechanisms of behavioral sensitization seen in rodents after repeated administration of psychostimulants, such as METH and amphetamine.

D-Serine is an endogenous co-agonist at the glycine-binding site of the NMDA receptor subunit, GluN1 [21–23]. D-Serine is synthesized from L-serine by the enzyme, serine racemase (SRR), and shows a similar localization within the brain to D-serine

[24,25]. Studies using *Srr* knockout (*Srr*-KO) mice show that SRR is predominantly localized to forebrain neurons [26] and that levels of D-serine in the forebrain are 10–20% of wild-type (WT) mice [27–29], suggesting that SSR provides the main catalysis for D-serine production in the forebrain. In addition, we reported that NMDA-induced neurotoxicity is significantly attenuated in the brains of *Srr*-KO mice, suggesting that D-serine controls the extent of NMDA receptor-mediated neurotoxic insults [27]. It is therefore likely that D-serine produced by SSR, plays an important role in NMDA receptor-mediated neurotransmission in the brain.

To study the role of SRR in METH-induced behavioral abnormalities, we evaluated behavioral performances in acute hyperlocomotion, development of behavioral sensitization, and conditioned place preference (CPP) in WT and *Srr*-KO mice, after the administration of METH. Furthermore, we examined the role of SRR on the dopamine (DA) release in the nucleus accumbens after administration of METH using *in vivo* microdialysis technique. In addition, we examined whether METH administration altered phosphorylation levels of ERK1/2 in the striatum, since ERK1/2 phosphorylation contributes to the development of behavioral sensitization by psychostimulants [30,31].

## Results

### METH-induced acute hyperlocomotion

A single dose of METH (3 mg/kg, s.c.), but not METH (1 mg/kg, s.c.), markedly increased locomotion in both WT and *Srr*-KO mice. Two-way ANOVA analysis revealed significant drug treatment effects for METH-induced locomotor responses [genotype: $F(1,48) = 1.12$, $p = 0.29$; drug treatment: $F(2,48) = 26.97$, $p<0.001$], with no genotype x drug treatment interaction ($F(2,48) = 0.27$, $p = 0.77$). Subsequent one-way ANOVA followed *post hoc* Bonferroni/Dun test indicated that METH (3 mg/kg) significantly increased locomotion in both WT and *Srr*-KO mice (WT: $p = 0.002$; *Srr*-KO: $p<0.001$ as compared to saline treated group) (**Figure 1**).

Next, we examined whether pretreatment with D-serine affected METH-induced acute hyperlocomotion in mice. Thirty minutes after a single oral dose of D-serine (900 mg/kg) or vehicle (10 ml/kg), mice were given a s.c dose of METH (3 mg/kg). Two-way ANOVA analysis revealed that D-serine had no significant effect on METH-induced acute hyperlocomotion [genotype: $F(1,24) = 6.00$, $p = 0.02$; drug treatment: $F(1,24) = 0.02$, $p = 0.88$; interaction: $F(1,24) = 0.02$, $p = 0.89$]. Student's t-test indicated that pretreatment with D-serine (900 mg/kg) had no effect on METH-induced hyperlocomotion in either WT or *Srr*-KO mice (WT: $t = 0.26$, $p = 0.80$; *Srr*-KO: $t = 0.006$, $p = 1.00$) (**Figure S1**).

### METH-induced behavioral sensitization

Two-way ANOVA analysis revealed a significant effect for METH-induced hyperlocomotion [genotype: $F(1,34) = 7.97$, $p = 0.008$; drug treatment: $F(1,34) = 33.46$, $p<0.001$; interaction: $F(1,34) = 11.83$, $p = 0.002$]. One-way ANOVA revealed a significant ($F(3,34) = 18.37$, $p<0.001$) difference among the four groups. Challenging mice with a low dose of METH (1 mg/kg) significantly ($p<0.001$) increased METH -induced hyperlocomotion in WT mice previously treated with METH (3 mg/kg/day over 5 consecutive days), compared with saline treated WT mice (**Figure 2**). In contrast, METH (1 mg/kg) -induced hyperlocomotion was comparable between *Srr*-KO mice previously treated with METH (3 mg/kg/day over 5 consecutive days) or saline (**Figure 2**), indicating a lack of METH-induced behavioral sensitization in *Srr*-KO mice. Furthermore, locomotion in WT mice pretreated with METH (3 mg/kg/day for 5 consecutive days) was significantly ($p = 0.001$) higher than seen in *Srr*-KO mice pretreated with METH (**Figure 2**). These results indicated that behavioral sensitization occurred in WT but not *Srr*-KO mice after repeated administration of METH.

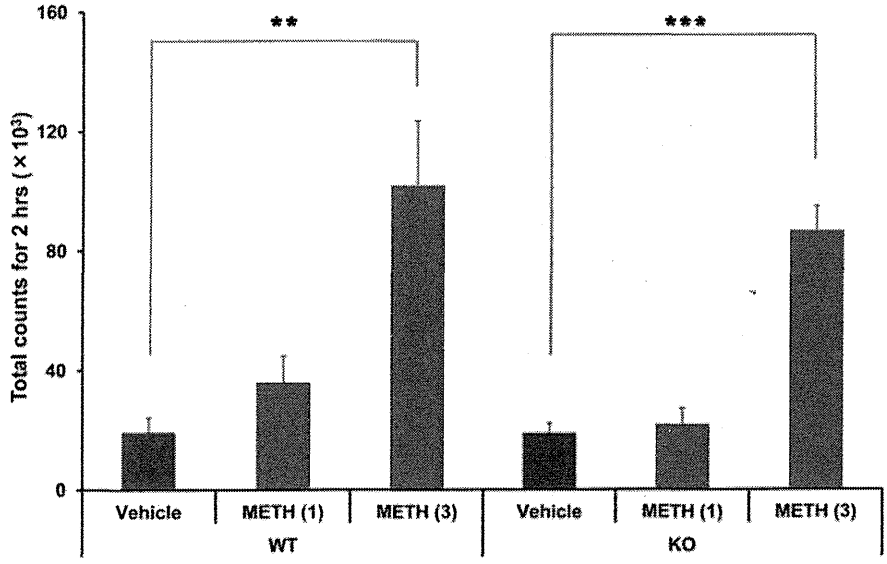


**Figure 1. METH-induced acute hyperlocomotion in WT and Srr-KO mice.** METH (1 or 3 mg/kg) or vehicle (saline; 10 ml/kg) was administered s.c. to WT and Srr-KO mice. Behavior (locomotion) was evaluated as described in the Methods and Materials. Each value is the mean ± SEM (n = 8–10 per group). **p<0.01, ***p<0.001 as compared with the vehicle treated group.
doi:10.1371/journal.pone.0035494.g001

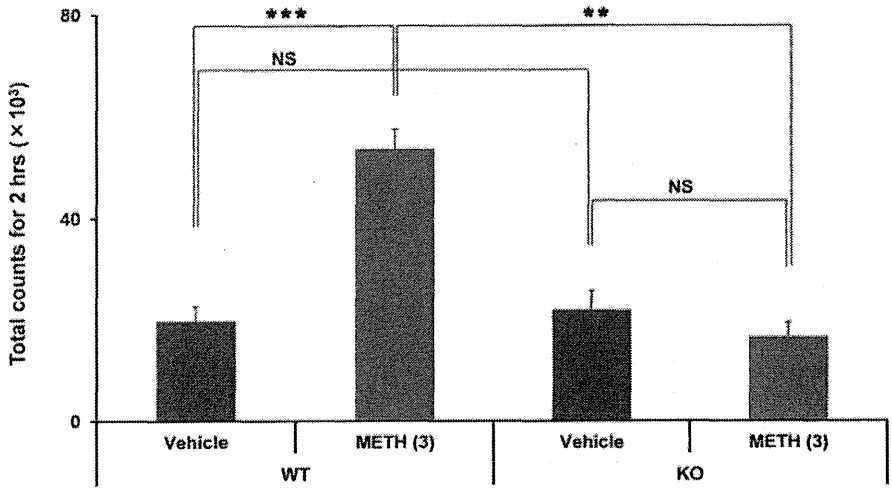


**Figure 2. The development of behavioral sensitization in mice after repeated administration of METH.** Mice were treated daily for 5 consecutive days with vehicle (10 ml/kg) or METH (3 mg/kg). Seven days after the final dosing, mice were given a lower dose of METH (1 mg/kg, s.c.). Locomotion in mice was evaluated as described in the Methods and Materials. Each value is the mean ± SEM (n = 9 or 10 per group). **p<0.01, ***p<0.001 as compared with the vehicle treated group (Bonferroni/Dunn method).
doi:10.1371/journal.pone.0035494.g002

To examine whether pretreatment with D-serine affected METH-induced behavioral sensitization in *Srr*-KO mice, mice were administered a single oral dose of D-serine (900 mg/kg/day) or vehicle (10 ml/kg/day) thirty minutes before dosing with METH (3 mg/kg/day). Two-way ANOVA analysis revealed a significant genotypic effect for METH-induced locomotion [genotype: $F(1,24) = 27.17$, $p<0.001$; drug treatment: $F(1,24) = 1.31$, $p = 0.26$], with no genotype x drug interaction ($F(1,24) = 0.21$, $p = 0.65$). One-way ANOVA revealed significant ($F(3,24) = 9.562$, $p<0.001$) differences among the four groups. Pretreatment with D-serine (900 mg/kg) showed no effect on METH (1 mg/kg)-induced locomotion in either WT or *Srr*-KO mice. In contrast, locomotion in WT mice pretreated with vehicle followed by METH (3 mg/kg) was significantly ($p = 0.015$) higher than in *Srr*-KO mice treated in the same way (**Figure S2**), consistent with results in **Figure 2**. Furthermore, locomotion in WT mice pretreated with D-serine (900 mg/kg) followed by a larger dose of METH (3 mg/kg) was significantly ($p = 0.003$) higher than in *Srr*-KO mice treated in the same manner (**Figure S2**). These results showed that pretreatment of D-serine (900 mg/kg) prior to each METH injection had no effect on METH (1 mg/kg)-induced locomotion in WT and *Srr*-KO mice pretreated with METH.

## METH-induced DA release in the nucleus accumbens

To explore how SRR contributes to METH-induced sensitization, we measured extracellular DA levels in the nucleus accumbens after administration of METH (1 mg/kg), using an *in vivo* microdialysis technique. A dose of METH (1 mg/kg, s.c.) caused a marked increase in extracellular DA levels in the nucleus accumbens of WT, not *Srr*-KO, mice previously treated with METH (3 mg/kg/day over 5 consecutive days) (**Figure 3**). Repeated ANOVA analysis showed a significant difference between two groups (Time×Group, $F = 3.456$, $p = 0.042$). The METH-induced DA release in the nucleus accumbes of *Srr*-KO mice previously treated with METH was significantly lower than that of WT mice previously treated with METH (**Figure 3**). These findings suggest that an administration of METH (1 mg/kg) failed to induce DA release in the nucleus accumbens of *Srr*-KO mice previously treated with METH.

## METH-induced rewarding effects

Mice that had only received METH spent significantly more time in the METH assigned compartment relative to the saline treatment compartment. The mice conditioned with saline did not show a preference for either compartment on the CPP test day. These data showed that a single pairing with METH (1 mg/kg, s.c.)-induced CPP when mice were tested 24 h after conditioning. Two-way ANOVA analysis revealed a significant drug treatment effect for the METH-induced CPP score [genotype: $F(1,40) = 0.37$, $p = 0.55$; drug treatment: $F(1,40) = 23.11$, $p<0.001$], with no genotype x drug treatment interaction ($F(1,40) = 0.44$, $p = 0.51$). Student's t-test indicated that repeated administration of METH (1 mg/kg) significantly increased CPP scores in both WT and *Srr*-KO mice (WT: $t = 3.71$, $p = 0.001$; *Srr*-KO: $t = 3.07$, $p = 0.006$) (**Figure 4**). The data indicated that METH treatment induced rewarding effects in both WT mice and *Srr*-KO mice.

## Phosphorylation of ERK1/2

ERK, a component of the mitogen-activated protein kinase (MAPK) intracellular signaling pathway, interacts with both dopamine and NMDA receptors in the brain. It has been reported that the phosphorylation of ERK1/2 plays a role in behavioral sensitization, after repeated administration of psychostimulants [30,31]. This study examined whether phosphorylation levels of ERK1/2 in the striatum of *Srr*-KO mice differed from that of WT mice. Two-way ANOVA analysis revealed a significant effect for METH-induced phosphorylation of ERK1/2 between WT and *Srr*-KO mice [ERK1; genotype: $F(1,20) = 0.07$, $p = 0.80$; drug treatment: $F(1,20) = 2.12$, $p = 0.16$; interaction: $F(1,20) = 6.13$, $p = 0.02$; ERK2; genotype: $F(1,20) = 0.16$, $p = 0.70$; drug treatment: $F(1,20) = 0.75$, $p = 0.40$; interaction: $F(1,20) = 12.89$, $p = 0.002$]. Student's t-test indicated that a single dose of METH (3 mg/kg) significantly increased the phosphorylation of ERK1/2 in the WT mice [ERK1; WT: $t = 2.61$, $p = 0.03$; ERK2; WT:

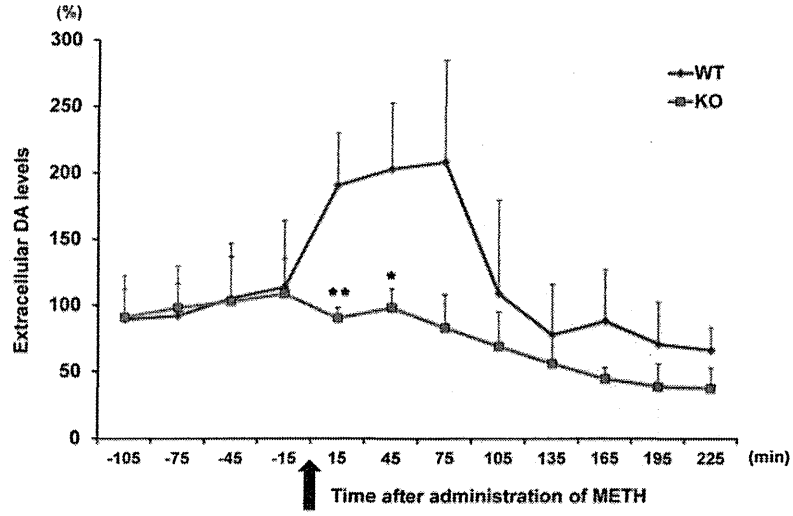


**Figure 3. The effects of SRR on METH-induced increase of extracellular DA levels.** A dose of METH (1.0 mg/kg, s.c) was injected into mice. The dialysate was collected in 30-min fractions, and DA levels were measured by HPLC. Basal extracellular DA levels in the nucleus accumbens were 3.841±0.301 nmol/L (n = 12, mean ± SEM). The values are the mean ± SEM of 6 mice. *p<0.05, **p<0.01 as compared with the METH (1 mg/kg) treated WT group (Student's t-test).
doi:10.1371/journal.pone.0035494.g003

t = 3.41, p = 0.006] (**Figure 5**). In contrast, a single dose of METH (3 mg/kg) did not increase phosphorylation of ERK1/2 in *Srr*-KO mice (ERK1; *Srr*-KO: t = 0.78, p = 0.46; ERK2; *Srr*-KO: t = 1.79, p = 0.10) (**Figure 5**).

In the hippocampus, two-way ANOVA analysis revealed no significant effect for METH-induced phosphorylation of ERK1/2 between WT and *Srr*-KO mice [ERK1; genotype: F (1,20) = 0.42, p = 0.53; drug treatment: F (1,20) = 0.23, p = 0.64; interaction: F (1,20) = 2.54, p = 0.13; ERK2; genotype: F (1,20) = 7.23, p = 0.01; drug treatment: F (1,20) = 1.61, p = 0.21; interaction: F (1,20) = 0.41, p = 0.53](**Figure S3**). In the frontal cortex, the phosphorylation of ERK1/2 was not detected between WT and *Srr*-KO mice (data not shown).

## Discussion

The major findings of this study are that repeated administration of METH (3 mg/kg/day for 5 days) induced behavioral

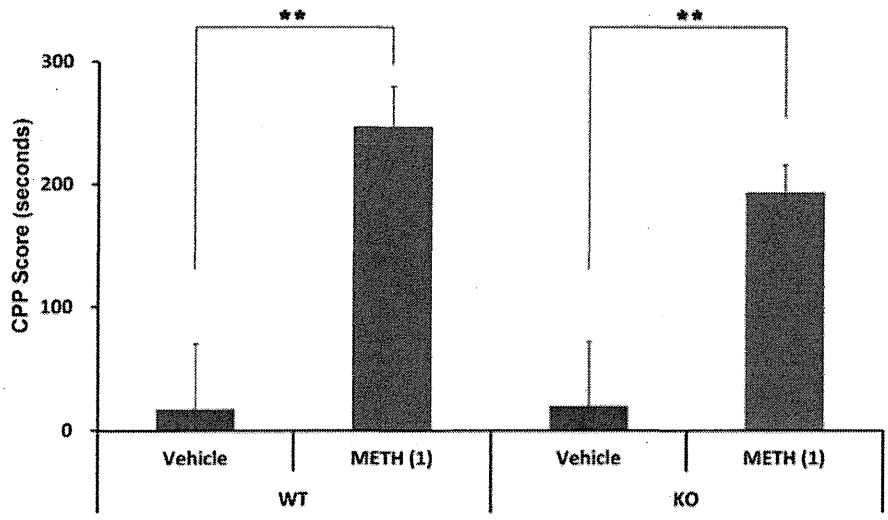


**Figure 4. METH-induced conditioned place preference (CPP) in mice.** On days 4, 6, and 8, mice were treated with vehicle (10 ml/kg) or METH (1 mg/kg), and then confined in either a transparent or black compartment for 30 min. On days 5, 7, and 9, mice were given saline and placed in the non- METH assigned compartment for 30 min. On day 10, the postconditioning test was performed as described in the Methods and Materials. Each value is the mean ± SEM (n = 11 per group). **p<0.01 as compared with the vehicle treated group (Student's t-test).
doi:10.1371/journal.pone.0035494.g004

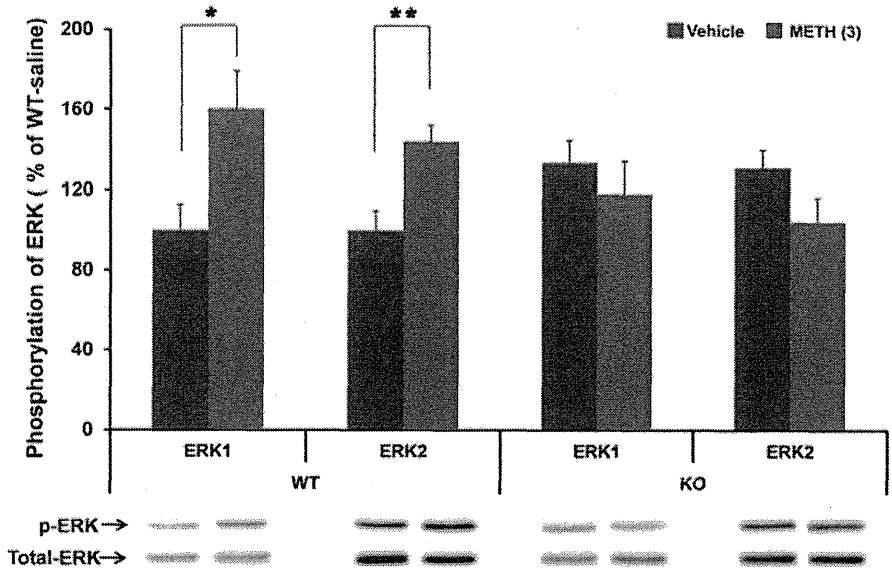


**Figure 5. Phosphorylation of ERK1/2 in the striatum after a single dose of METH.** Mice were sacrificed 15 minutes after a single dose of either METH (3 mg/kg, s.c.) or vehicle (10 ml/kg, s.c.). Western blot analysis of phospho-ERK1/2 and total ERK1/2 protein was performed as described in the Methods and Materials. Values are the mean ± S.E.M. (n = 6 per group). *p<0.05, **p<0.01 as compared with the vehicle treated group (Student's t-test).
doi:10.1371/journal.pone.0035494.g005

sensitization in WT mice, but not *Srr*-KO mice, and that a single dose of METH (3 mg/kg) produced the same changes in acute hyperlocomotion between *Srr*-KO and WT mice. From *in vivo* microdialysis, we found that METH-induced DA release in the nucleus accumbens of *Srr*-KO mice previously treated with METH (3 mg/kg/day over 5 consecutive days) was significantly attenuated as compared with WT mice previously treated with METH (3 mg/kg/day over 5 consecutive days). To our knowledge, this is the first report demonstrating the role of SRR in the development of METH-induced behavioral sensitization. Previously, we reported that levels of D-serine in the forebrain of *Srr*-KO mice were reduced to approximately 10–20% of those found in WT mice [27,29]. However, pretreatment with D-serine (900 mg/kg) did not alter hyperlocomotion in WT and *Srr*-KO mice after a single dose of METH (3 mg/kg), suggesting that decreased levels of D-serine in the brain do not affect METH-induced, acute hyperlocomotion in mice. Furthermore, pretreatment with D-serine (900 mg/kg/day) prior to each METH injection, failed to induce behavioral sensitization in *Srr*-KO mice. It is therefore unlikely that pretreatment with D-serine affects METH-induced behavioral abnormalities in either WT or *Srr*-KO mice. These findings suggest that SRR plays an important role in the development of behavioral sensitization in mice, following repeated METH administration.

Behavioral sensitization following the repeated administration of psychostimulants, including METH, is one manifestation of sensitization in the brain. The initiation of behavioral sensitization to psychostimulants is operationally defined as the transient sequence of cellular and molecular events precipitated by repeated administration of psychostimulants that leads to the enduring changes in neural function responsible for behavioral augmentation [14,15,32,33]. The increase in extracellular DA is augmented in the nucleus accumbens and striatum following the repeated administration of psychostimulants. Together, the enhanced release of DA in the nucleus accumbens plays a role in the augmentation of behavior in the sensitized animals [14,15,32,33]. In this study, we found that *Srr*-KO mice pretreated with METH did not show the release of DA in the nucleus accumbens and behavioral augmentation after a challenge of METH, indicating a role of *Srr* in the development of behavioral sensitization after repeated administration of METH.

Accumulating evidence suggests that intracellular signaling pathways, including that of ERK1/2 play contributes greatly to the molecular pathophysiology of drug addiction [34–38]. Abused drugs including amphetamine and cocaine has been shown to activate ERK in a subset of medium-sized spiny neurons of the dorsal striatum and nucleus accumbens, through the combined action of NMDA and DA $D_1$ receptors [39–41]. Pretreatment with SL327 (30 mg/kg), a selective brain-penetrating inhibitor of MAP-kinase/ERK kinase, blocks the development of behavioral sensitization after repeated amphetamine treatment [39], suggesting a role for this pathway in long-lasting behavioral sensitization by psychostimulants. It has also been shown that phosphorylation of ERK1/2 in the striatum increases after administration of psychostimulants [30,31,40–41]. In this study, a single dose of METH (3 mg/kg) significantly increased the phosphorylation of ERK1/2 in the striatum of WT, but not *Srr*-KO mice. This suggests that phosphorylation of ERK1/2 in the striatum following a single dose of METH, is at least in part, mediated by SRR, although the precise mechanisms are currently unclear. Previously, we reported that NMDA-induced neurotoxicity is significantly attenuated in the brains of *Srr*-KO mice, suggesting that D-serine controls the extent of NMDA receptor-mediated neurotoxic insults [27]. It is likely that the lack of behavioral sensitization seen in *Srr*-KO mice may be the result of decreased DA release and ERK1/2 phosphorylation, due to NMDA receptor hypofunction, although this will need to be investigated further.

The CPP paradigm is a widely used animal model on the rewarding effects of drugs [42]. The NMDA receptor antagonist MK-801 fails to block amphetamine-induced place preference in rats, suggesting that NMDA receptors may not be involved in the rewarding effects of psychostimulants [43]. Miyamoto et al. [44] reported that mice with mutant GluN2A, one of four GluN2 subunits (GluN2A-D) of the NMDA receptor, developed METH-induced place preference to the same degree as WT mice, whereas behavioral sensitization was significantly reduced in these mutants compared with WT mice. This suggests that the GluN2A subunit may play a role in the development of behavioral sensitization, but not rewarding effects, in mice repeated exposure to METH. In this study, *Srr*-KO mice developed METH-induced place preference to the same degree as WT mice. It is therefore unlikely that NMDA receptors play a major role in the development of METH-induced rewarding effects in mice.

Along with D-serine, glycine is also a co-agonist at the glycine modulatory site of the NMDA receptor [21]. We reported that brain derived levels of glycine and other amino acids, including, glutamate and glutamine, were comparable between WT and *Srr*-KO mice [27,29], suggesting that glycine may not compensate for decreased D-serine levels in the brains of *Srr*-KO mice. In addition, forebrain levels of the NMDA subunits, GluN2A, GluN2B, and GluN1 were comparable between WT and *Srr*-KO mice [27]. No difference was found in [$^3$H](+)-MK-801 binding between brain regions (frontal cortex, hippocampus, striatum, cerebellum) from WT and *Srr*-KO mice (**Table S1**). It would seem that the expression of NMDA receptors is comparable between WT and *Srr*-KO mice. It is highly probable that the reduced D-serine in the forebrain of *Srr*-KO mice may, in part, contribute to the lack of METH-induced behavioral sensitization, although this too needs to be examined in further studies.

In conclusion, this study has pointed to a role for SRR in the development of behavioral sensitization, but not rewarding effects, in mice that have been repeatedly exposed to METH. It also suggests that decreased DA release in the nucleus accumbens and decreased phosphorylation of the ERK1/2 protein may contribute to the lack of METH-induced behavioral sensitization in *Srr*-KO mice.

## Materials and Methods

### Animals

*Srr*-KO mice were generated from C57BL/6- derived embryonic stem cells transfected with a gene-targeting vector containing C57BL/6 mouse genomic DNA, and the colony was expanded by crossing with C57BL/6 mice [26]. The generation and genotyping of *Srr*-KO and WT mice with a pure C57BL/6 genetic background has been reported previously [26]. WT and *Srr*-KO mice aged 2–3 months were used for all behavioral studies. The mice were housed in clear polycarbonate cages (22.5×33.8×14.0 cm) in groups of 5 or 6 per cage, under a controlled 12/12-h light–dark cycle (lights on from 7:00 AM to 7:00 PM), with a room temperature of 23±1°C and humidity at 55±5%. The mice were given free access to water and food pellets. The experimental procedure (Permit Number: #23-151) was approved by the Animal Care and Use Committee of Chiba University.

### Drug Administration

METH (D-methamphetamine hydrochloride) was purchased from Dainippon-Sumitomo Pharmaceutical Ltd., (Osaka, Japan) and D-serine from Sigma-Aldrich Corporation (St. Louis, MO). METH was dissolved in physiological saline and injected subcutaneously (s.c.). The dose of METH was expressed as a hydrochloride salt. D-Serine dissolved in saline was administered orally at a concentration of 900 mg/kg of body weight. Other chemicals were purchased from commercial sources.

### METH-induced Acute Hyperlocomotion

METH (1 and 3 mg/kg) or a vehicle of physiological saline (10 ml/kg) was administered s.c. into mice. Locomotor activity was measured using an animal movement analysis system (SCANET SV-10, Melquest, Toyama, Japan), as reported previously [45–47]. The system consisted of a rectangular enclosure (480×300 mm). The side walls (height, 60 mm) of the enclosure were equipped with 144 pairs of photosensors located 30 mm from the bottom edge and at 5 mm intervals. Recordings were taken from single animals. A pair of photosensors was scanned every 0.1 s to detect the animal movement. The intersection of paired photosensors (10 mm apart) in the enclosure was counted as one unit of locomotor activity. Data was collected for 180 min (60 min of habituation and for 120 min after the injection of METH or saline). To examine the role of D-serine in METH-induced acute hyperlocomotion, animals were pretreated with D-serine, before administration of METH. Thirty minutes after a single oral dose of D-serine (900 mg/kg) or vehicle (10 ml/kg), mice were administered a dose of METH (3 mg/kg, s.c). Locomotor activity was measured using the animal movement analysis system (SCANET SV-10, Melquest, Toyama, Japan), described above.

### METH-induced Behavioral Sensitization

Wild type and *Srr*-KO mice were given a single s.c. dose of vehicle (10 ml/kg) or METH (3 mg/kg), and returned to their home cages. This process was repeated for each animal, over 5 consecutive days. One week after the final treatment, each mouse was given a low dose of METH (1 mg/kg, s.c.), and behavioral changes (locomotion) were measured using the animal movement analysis system (SCANET SV-10, Melquest, Toyama, Japan), described above.

Next, mice were pretreated with D-serine in order to examine its role in METH-induced behavioral sensitization. Both WT and *Srr*-KO mice were treated with either: vehicle (10 ml/kg) + METH (3 mg/kg) group or D-serine (900 mg/kg) + METH (3 mg/kg) group. Injections were given 30 min apart. After the administration of METH, mice were returned to their home cages and this treatment was repeated over 5 consecutive days. One week after the final treatment, all mice were given a low dose of METH (1 mg/kg, s.c.), and behavioral changes (locomotion) were measured using the animal movement analysis system (SCANET SV-10, Melquest, Toyama, Japan), described above.

### Measurement of extracellular DA levels using *in vivo* microdialysis

Mice were anesthetized with sodium pentobarbital prior to the stereotaxic implantation of a probe into the nucleus accumbens (+1.1 mm anteroposterior, +1.0 mm mediolateral from the bregma, and −4.0 mm dorsoventral from the dura), according to the Franklin and Paxinos Atlas [48], as reported previously [49]. Probes were secured onto the skull using stainless-steel screws and dental acrylic. Twenty-four hours after surgery, *in vivo* microdialysis was performed on conscious and free moving mice. Probes were perfused continuously with artificial CSF (147 mM NaCl, 4 mM KCl, and 2.3 mM $CaCl_2$) at a rate of 2 µl/min. METH (1 mg/kg, s.c.) was administered into mice. The dialysate was collected in 30-min fractions. After *in vivo* microdialysis experi-